OAK RIDGE NATIONAL LABORATORY LIBRARIES
3 4456 0550293 4

CENTRAL RESEARCH LIBRARY

ORNL-TM-4349

cy. 71

RESPONSE OF A LARGE ALL-LIQUID SCINTILLATION SPECTROMETER AND OF A 24-LAYER IRON-PLASTIC SPECTROMETER TO CHARGED PIONS AND PROTONS IN THE LOW-GEV ENERGY RANGE

T. A. Gabriel
J. D. Amburgey

OAK RIDGE NATIONAL LABORATORY
CENTRAL RESEARCH LIBRARY
DOCUMENT COLLECTION
LIBRARY LOAN COPY
DO NOT TRANSFER TO ANOTHER PERSON
If you wish someone else to see this document, send in name with document and the library will arrange a loan.
UCN-7969
(3 3-67)

OAK RIDGE NATIONAL LABORATORY
OPERATED BY UNION CARBIDE CORPORATION • FOR THE U.S. ATOMIC ENERGY COMMISSION

This report was prepared as an account of work sponsored by the United States Government. Neither the United States nor the United States Atomic Energy Commission, nor any of their employees, nor any of their contractors, subcontractors, or their employees, makes any warranty, express or implied, or assumes any legal liability or responsibility for the accuracy, completeness or usefulness of any information, apparatus, product or process disclosed, or represents that its use would not infringe privately owned rights.

ORNL-TM-4349

Contract No. W-7405-eng-26

Neutron Physics Division

RESPONSE OF A LARGE ALL-LIQUID SCINTILLATION SPECTROMETER AND OF A 24-LAYER IRON-PLASTIC SPECTROMETER TO CHARGED PIONS AND PROTONS IN THE LOW-GEV ENERGY RANGE*

T. A. Gabriel and J. D. Amburgey†

*Submitted for journal publication.

†Computer Sciences Division of the General Staff.

DECEMBER 1973

NOTICE This document contains information of a preliminary nature and was prepared primarily for internal use at the Oak Ridge National Laboratory. It is subject to revision or correction and therefore does not represent a final report.

OAK RIDGE NATIONAL LABORATORY
Oak Ridge, Tennessee, 37830
operated by
UNION CARBIDE CORPORATION
for the
U. S. ATOMIC ENERGY COMMISSION

OAK RIDGE NATIONAL LABORATORY LIBRARIES

3 4456 0550293 4

RESPONSE OF A LARGE ALL-LIQUID SCINTILLATION SPECTROMETER AND OF A 24-LAYER IRON-PLASTIC SPECTROMETER TO CHARGED PIONS AND PROTONS IN THE LOW-GEV ENERGY RANGE

T. A. Gabriel and J. D. Amburgey

Oak Ridge National Laboratory
Oak Ridge, Tennessee, 37830

Abstract

To aid in the design of a particular class of ionization spectrometers, calculations have been carried out to determine the response of a large all-liquid scintillation spectrometer to incident protons and charged pions in the low-GeV energy range. Included for comparative purposes is the calculated response of a 24-layer iron-plastic sandwich spectrometer of comparable gram/cm^2 thickness. The calculated data include spatially dependent energy deposition, spatially integrated contributions to the total energy deposition, leakage and binding energies, scintillation pulse-height distributions including and excluding saturation effects, and correlations between different variables. Also included for several cases is the calculated Cerenkov response.

1. INTRODUCTION

To aid in the design of certain scintillation spectrometers, calculations have been carried out to determine the response of a large all-liquid organic scintillation spectrometer to incident protons and charged pions in the low-GeV energy range. The spectrometer used in the calculations is cylindrical in shape with a diameter of 254 cm and a length of 355.6 cm. The composition is CH_2 with a density of 0.87 g/cm^3. For comparison, the response of a 24-layer iron-plastic scintillation spectrometer of comparable g/cm^2 thickness has also been calculated.

The calculational techniques, which were previously proven to be valid[1]), were applied to the present calculations. These techniques provide in detail the energy deposition produced by the hadron and electromagnetic cascades which occur when the incident particle interacts within the spectrometer and a means of conversion from energy deposition to scintillation light through the use of Birks' law[2]). The data include spatially dependent energy deposition, spatially integrated contributions to the energy deposition, leakage and binding energies, pulse-height distributions including and excluding saturation effects (Birks' law), and various scatter plots which yield correlations between different variables such as binding energy, energy deposition, etc. Also included for several cases are the calculated Cerenkov responses and the correlation between Cerenkov and scintillation responses. The calculational methods are described in Sec. 2 and the results are presented and discussed in Sec. 3.

2. METHOD OF CALCULATION

The three-dimensional, high-energy nucleon-meson transport code HETC[3]) was used to obtain a detailed description of the nucleon-meson cascade produced in each of the energy-absorbing devices. This Monte Carlo code takes into account the slowing down of charged particles (via the continuous slowing-down approximation), the decay of charged pions and muons, nonelastic nucleon- and charged-pion-nucleus (excluding hydrogen) collisions [through the intranuclear-cascade-evaporation model[4]) ($E \leqslant 3$ GeV) and the extrapolation-evaporation model[5]) ($E \geqslant 3$ GeV)], nonelastic nucleon- and charged-pion-hydrogen collisions [via the isobar model[6]) ($E \leqslant 3$ GeV) and phenomenological fits to experimental data[7]) ($E \geqslant 3$ GeV)], elastic neutron-nucleus collisions ($E \leqslant 100$ MeV), and elastic nucleon- and charged-pion collisions with hydrogen. In most applications using HETC, nucleons are transported to 15 MeV and charged pions are transported to ~ 2 MeV, with negative pions being captured when they slow down to their cut-off energy. In the present application, neutrons below 15 MeV (below 10 MeV in the iron-plastic spectrometer) were assumed to deposit their energy at their point of origin. In applications where the transport of the low-energy neutrons is important, the three-dimensional multigroup neutron and gamma-ray Monte Carlo transport code MORSE[8]) or the three-dimensional neutron Monte Carlo transport code O5R[9]) are used. (MORSE has been utilized in this paper for two cases to check the assumption concerning the low-energy neutrons.)

The source distribution for the electromagnetic-cascade calculation, i.e., photons from neutral-pion decay and electrons and positrons from muon decay, is provided by HETC. The transport of these particles was carried out using a modified version of the Monte Carlo code developed by Beck[10]). This code takes into account most of the significant electron-, positron-, and photon-interaction processes, i.e., Compton scattering, pair production, bremsstrahlung, photoelectric effect, annihilation, and the slowing down of electrons and positrons due to ionization and excitation.

The two major modifications of the original code are: (1) the change from a one-medium transport code to a multimedium transport code, and (2) the inclusion of a more generalized geometry package so that a three-dimensional transport calculation can be performed. For all processes except Compton scattering, however, the products of an interaction are assumed to be emitted in the same direction as the particle producing the interaction.

Gamma rays from the decay of excited nuclei following a nuclear interaction were not transported in the present calculations but were assumed to have deposited their energy at their point of origin. This is a fairly good approximation since a large portion of the electromagnetic-cascade source energy for the problems considered here results from neutral pions. Also, since most de-excitation photons are of low energy, they are rapidly absorbed by the media.

The nonlinearity of the light pulse (i.e., the light observed is not in direct proportion to the energy deposited due to saturation) has been taken into account by the use of Birks' law[2]):

$$\frac{dL}{dx} = \frac{dE/dx}{1+kB\ dE/dx} \quad \text{or} \quad L(E_2) - L(E_1) = \int_{E_1}^{E_2} \frac{dE}{1+kB\ dE/dx} \quad . \qquad (1)$$

The light curves corresponding to several particles at low energies for the media indicated are shown in fig. 1 for kB = 0.01 g/cm^2/MeV. In the calculation, the light curves were extended to the maximum necessary energy. The ionization energy loss, dE/dx, used in evaluating eq. 1, was taken from a program due to Armstrong and Chandler[11]). It has been assumed that for electrons and positrons a linear relation holds between the light observed and the energy deposited; i.e., L = E. This is a very good approximation for all electron energies above 0.1 MeV.

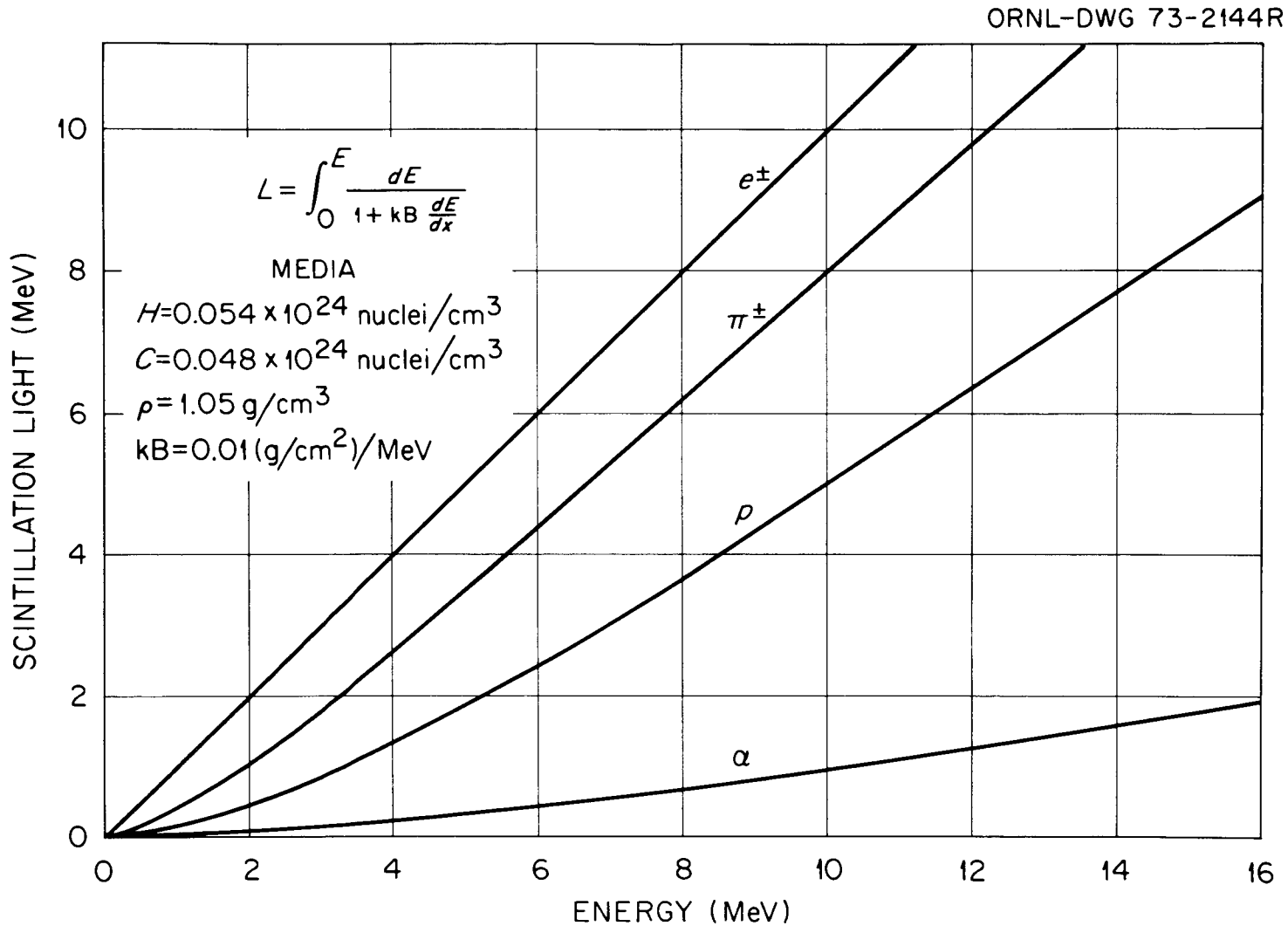

Fig. 1. Scintillation light output vs energy for several different types of particles.

Neutrons with energies < 15 MeV (< 10 MeV for the iron-plastic spectrometer) were assumed to lose all their energy at their point of origin and to produce light in the scintillating material through proton recoil. Since low-energy neutrons produce a small fraction of the light observed, this is a good approximation. In addition, the light produced by the residual excitation energy which remains in a nucleus following a nuclear interaction and which is emitted in the form of gamma rays was assumed to be directly proportional to the energy available.

The Cerenkov response of this device, which is considerably weaker than the scintillation response and which is useful only when other modes of light emission are extremely small, can be obtained from the following equations:

$$\frac{dI}{dx} = \frac{4\pi^2 e^2 Z^2}{hc^2} \Delta\nu \left(1 - \frac{1}{\beta^2 n^2}\right)$$

or

$$I = \int_{E_{THRESHOLD}}^{E} \frac{4\pi^2 e^2 Z^2}{hc^2} \Delta\nu \left(1 - \frac{1}{\beta^2 n^2}\right) \frac{dE}{dE/dx} ,$$

where

$\frac{dI}{dx}$ = the number of photons emitted per centimeter,

$\Delta\nu$ = the frequency interval of the photons,

Z = the charge of the particle,

$E_{THRESHOLD}$ = the threshold energy for emitting Cerenkov radiation,

β = the velocity of the particle relative to light velocity c,

n = the index of refraction of the medium in the frequency interval considered,

dE/dx = the ionization and excitation energy loss, and

e,h,c = the electronic charge, Plank's constant, and the speed of light, respectively.

In the calculations, $\Delta\nu$ has been taken to be 2.9×10^{14} sec^{-1}, which corresponds roughly to the frequency range of the visible spectrum, and n has been taken to be 1.5. Also, the number of photons has been converted to electrons by assuming an average photocathode efficiency in the $\Delta\nu$ frequency range of 0.06, i.e., 0.06 electron/photon. The Cerenkov radiation curves for the media indicated are shown in fig. 2. Charged particles with $A > 1$ are not considered since the number of these particles having energies above their Cerenkov threshold energies is negligible. The charged-muon response is not plotted but corresponds very closely to the curve for the charged pions. In the calculations, the Cerenkov radiation curves were extended from threshold to the maximum necessary energy.

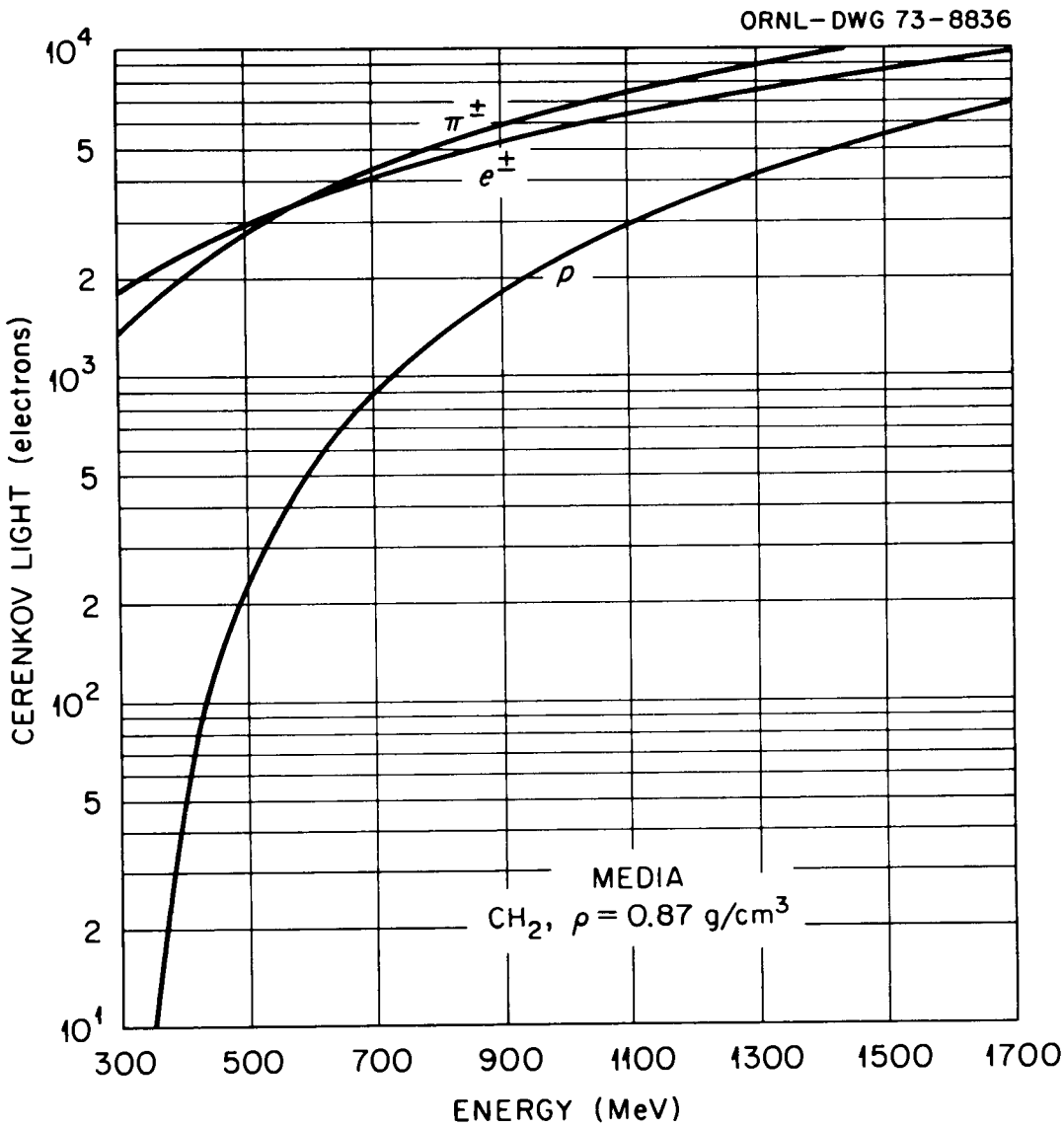

Fig. 2. Cerenkov light output vs energy for several different types of particles.

3. RESULTS

The dimensions and composition of the all-liquid organic scintillation spectrometer used in the calculations are shown in fig. 3. In all of the calculations, the incident beam is assumed to enter at the center of and perpendicular to the front face.* Calculated results for 1-GeV/c incident π^- are summarized in figs. 4-12 and in tables 1-3. The spatial distribution of the total energy deposition as a function of depth in the spectrometer is given in fig. 4 for several radial intervals. In table 1 complete data for the spatial energy deposition are given. The numbers below the tabulated data represent the statistical errors in percent for one standard deviation. The spatially integrated energy deposition (linear) in several categories and the leakage energy as to particle type and region of escape are given in table 2. As can be seen from this table, the major modes of energy deposition are from primary ionization, secondary pion ionization, secondary proton ionization, and from the electromagnetic cascade initiated from the decay of the π^0's. The data in the table also indicate that the major modes of leakage energy are from neutrons with energies > 15 MeV and from γ-rays. Even though the device is quite large, the low average Z of the material is ineffective in converting the γ-rays to e^- and e^+ pairs.

To check the assumption concerning the neutrons with energies < 15 MeV (i.e., the low-energy neutrons were assumed to deposit their energy within the device), a transport calculation was performed using the code MORSE[8]) to obtain the amount of low-energy neutron leakage. Of the possible 15.9 MeV of neutron energy that could leak out, less than 3% did. This good containment of the low-energy neutrons is a direct consequence of the large amount of hydrogen contained within the system. Also given in the table are the electromagnetic source energy and the binding energy plus neutrino energy. The latter quantities were obtained through an energy balance.

*This is not a limitation of the calculation as arbitrary geometric orientations are possible.

ORNL-DWG 73-9899

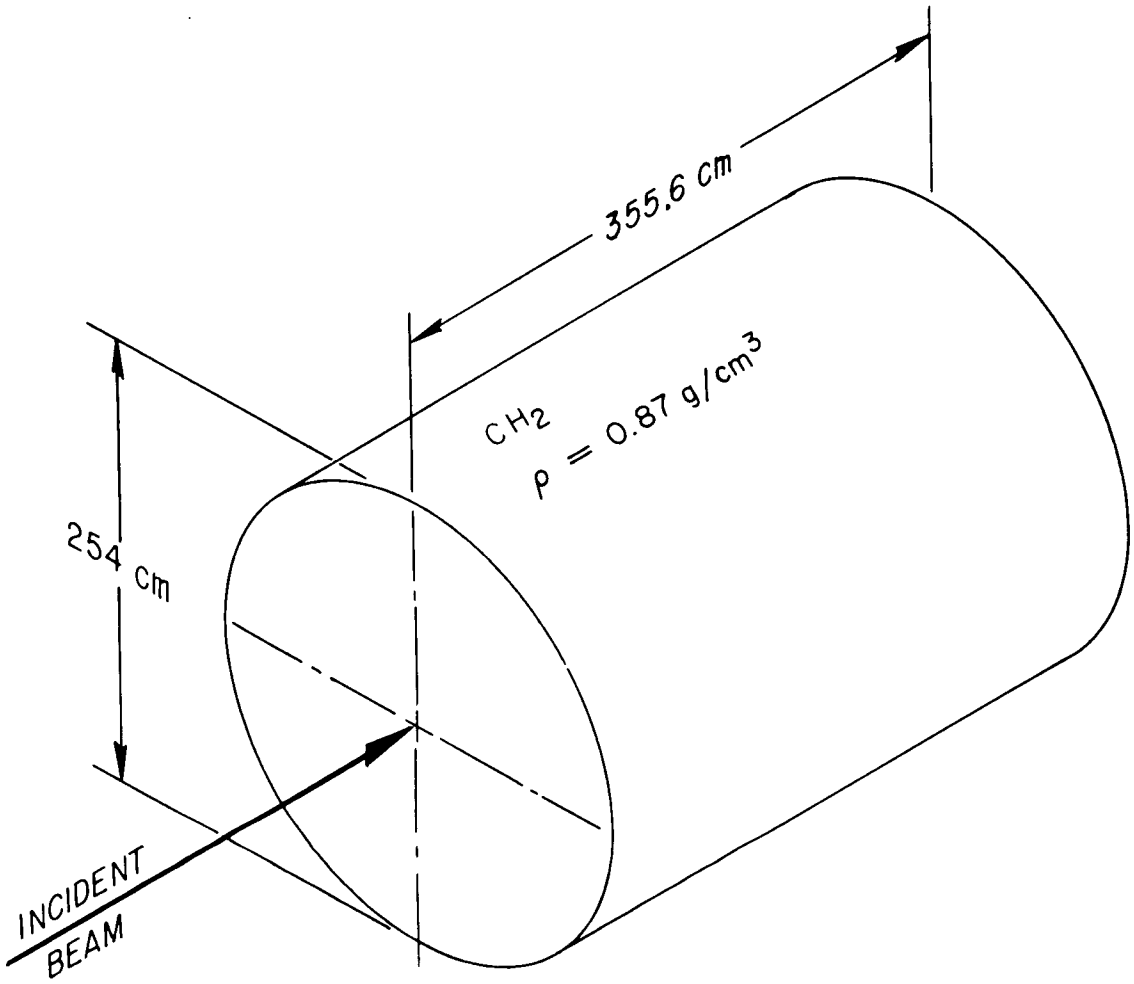

Fig. 3. Geometry and composition of the large scintillation spectrometer.

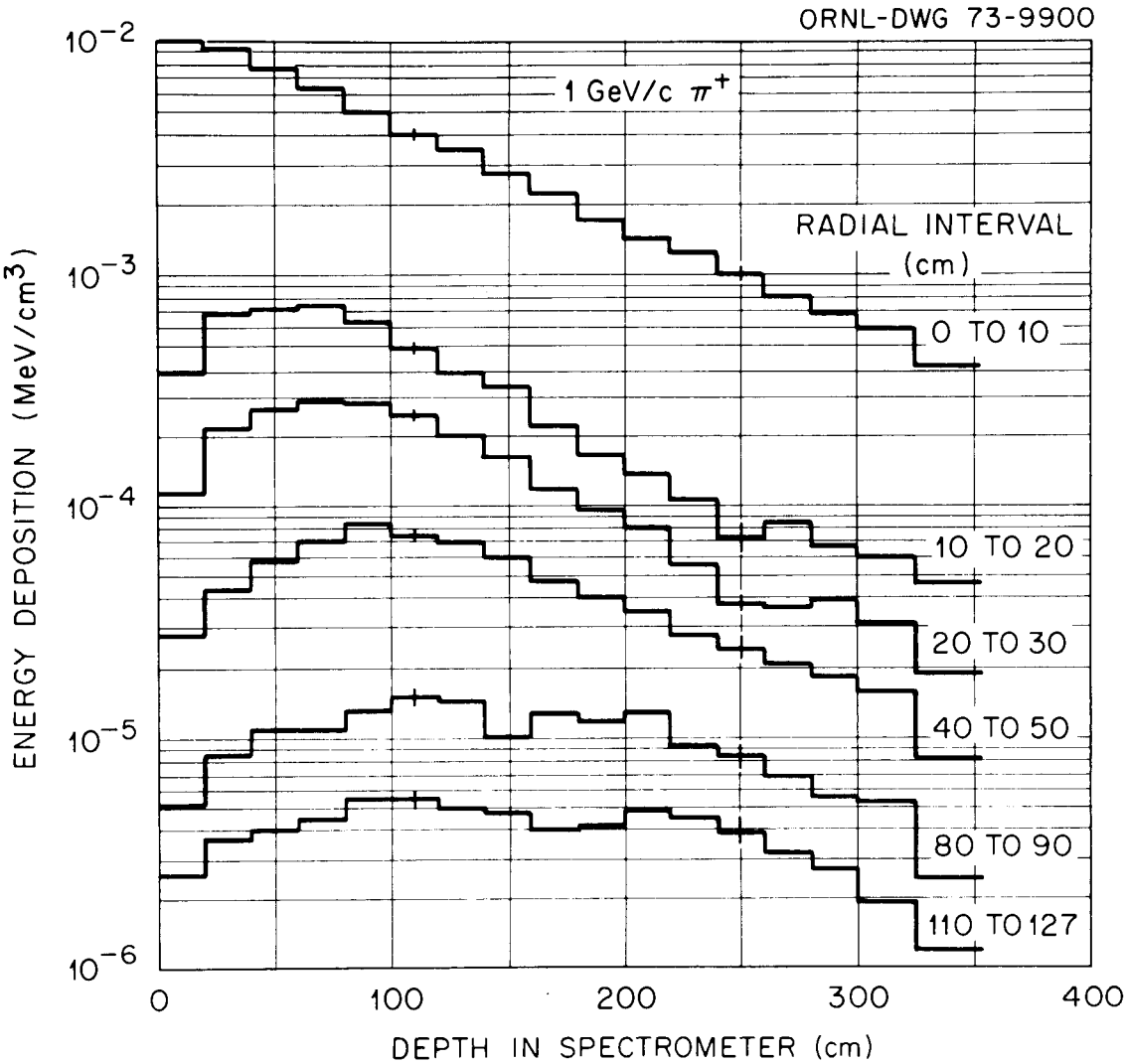

Fig. 4. Spatial distribution of the energy deposition produced by the interaction of 1-GeV/c π^+ in a large scintillation spectrometer.

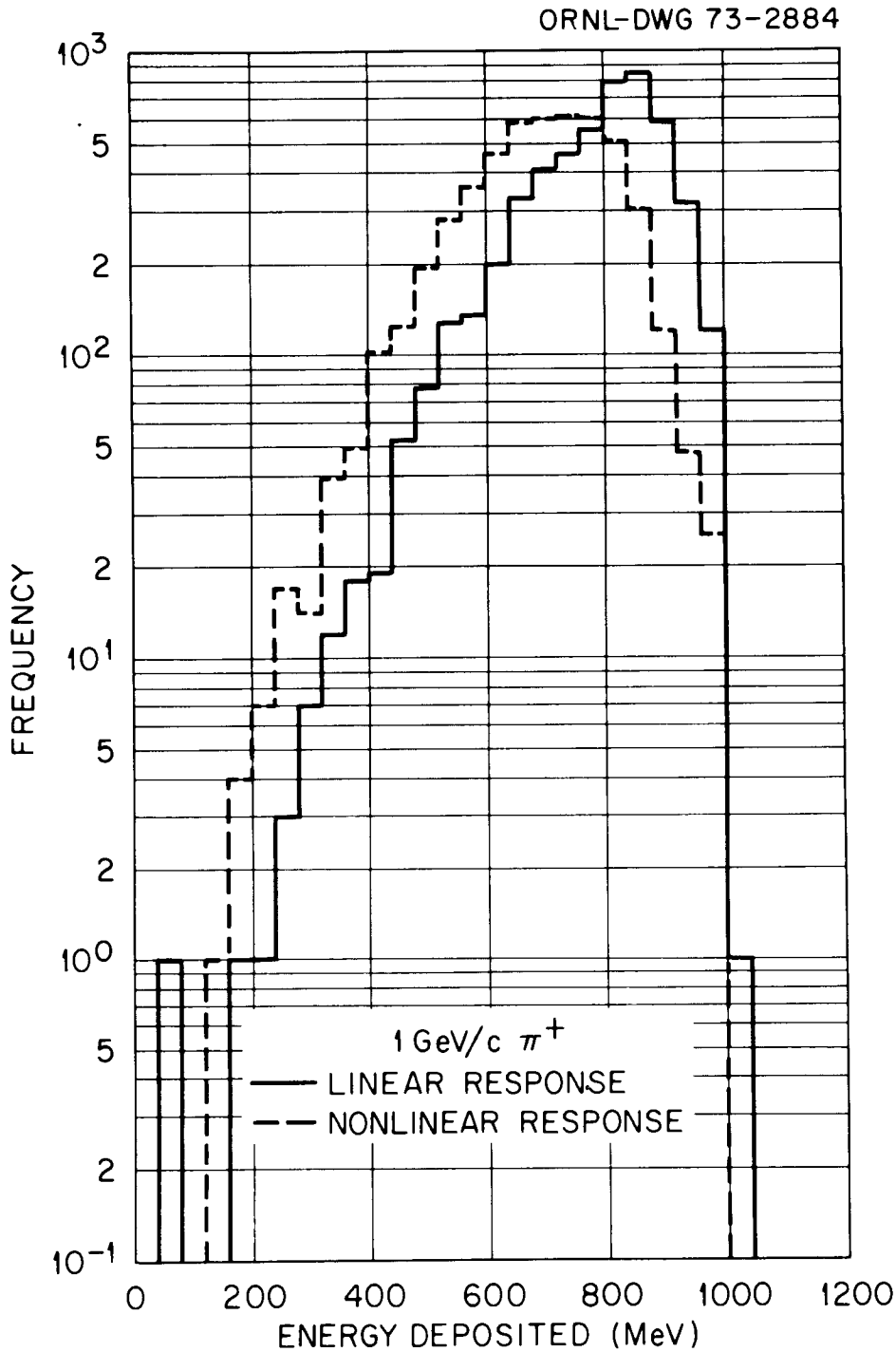

Fig. 5. Linear and nonlinear scintillation pulse-height distributions for incident 1-GeV/c π^+.

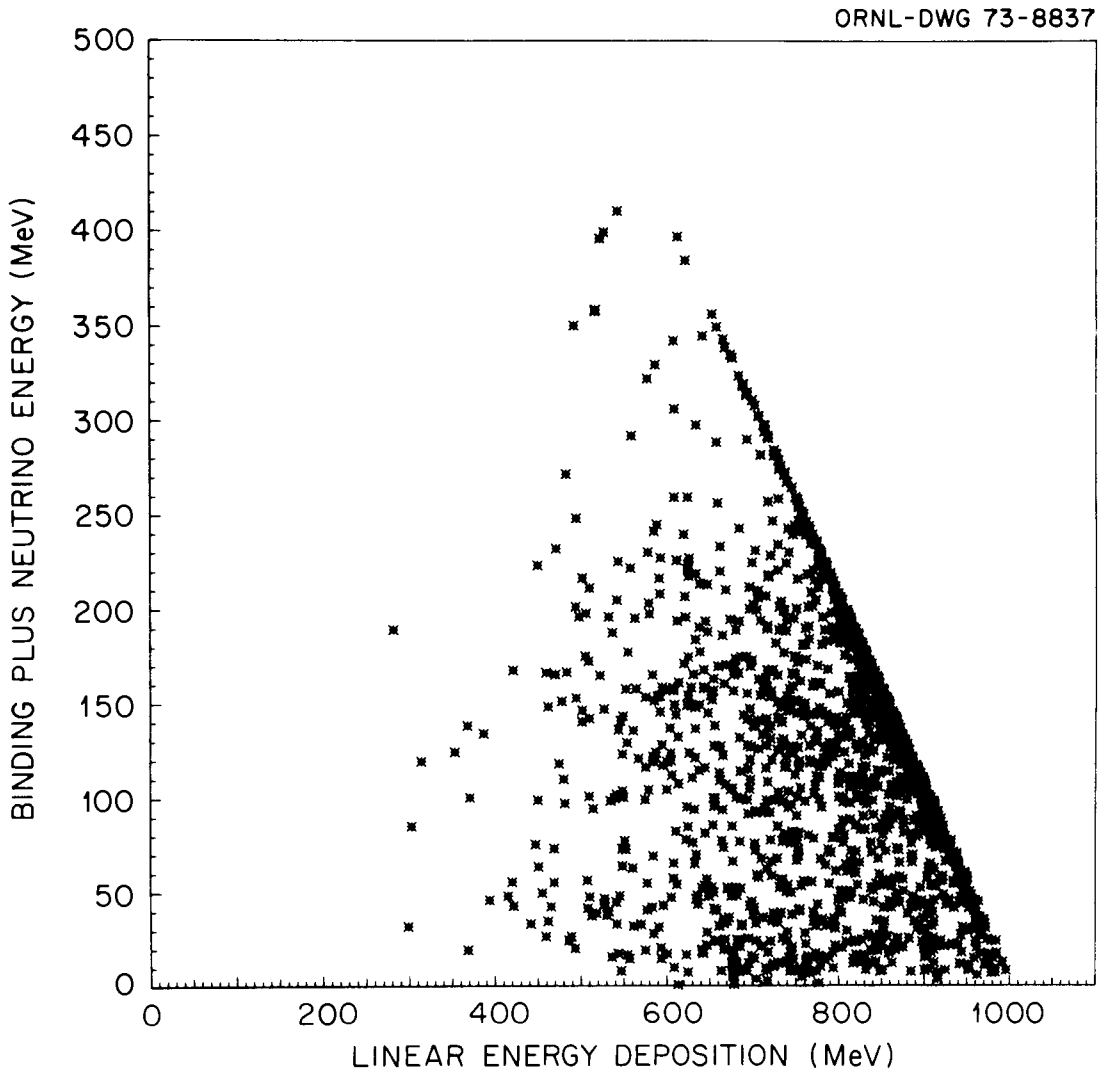

Fig. 6. Scatter plot of binding plus neutrino energy vs linear energy deposition for incident 1-GeV/c π^+.

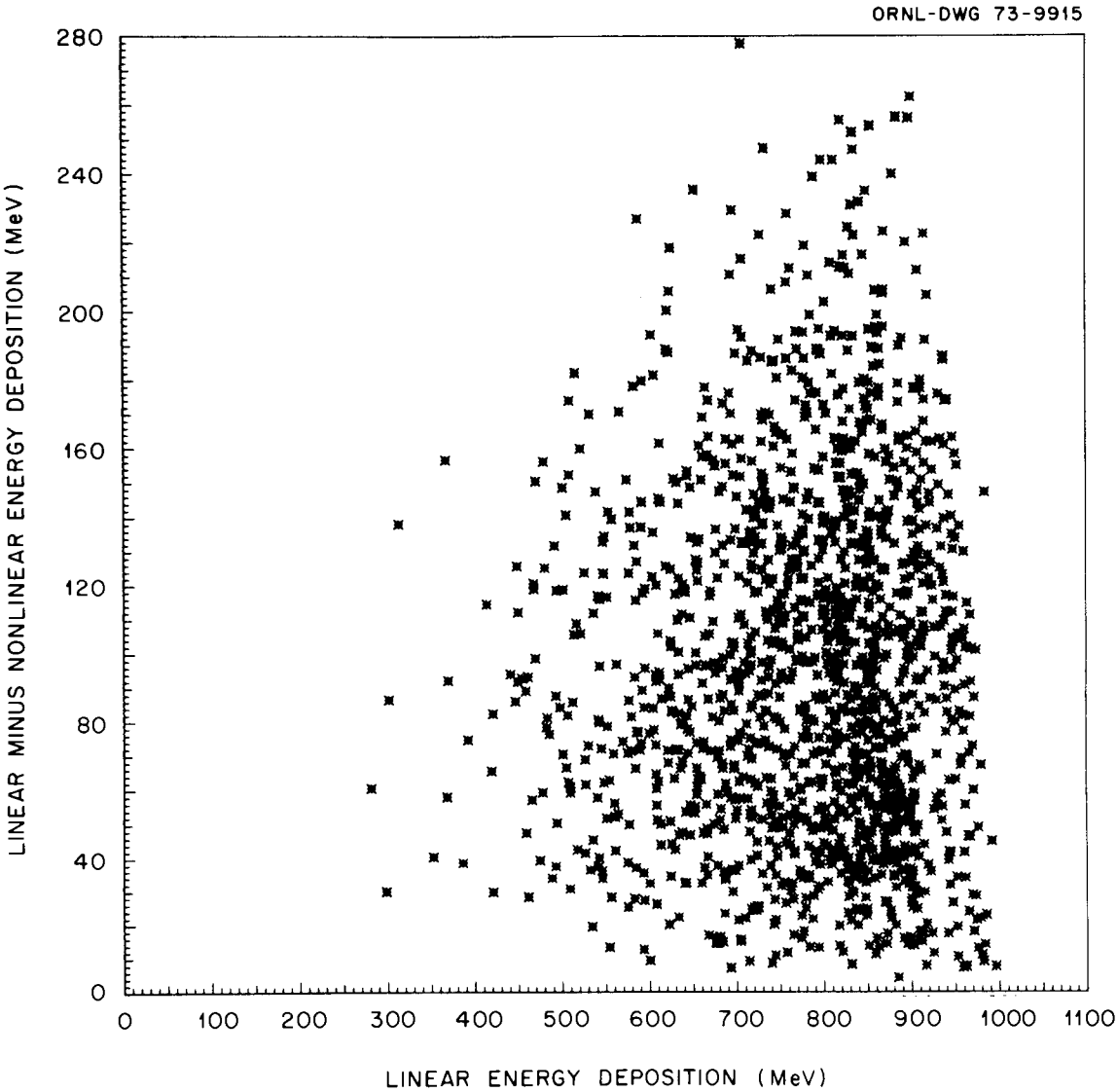

Fig. 7. Scatter plot of linear minus nonlinear energy deposition vs linear-energy deposition for 1-GeV/c π^+.

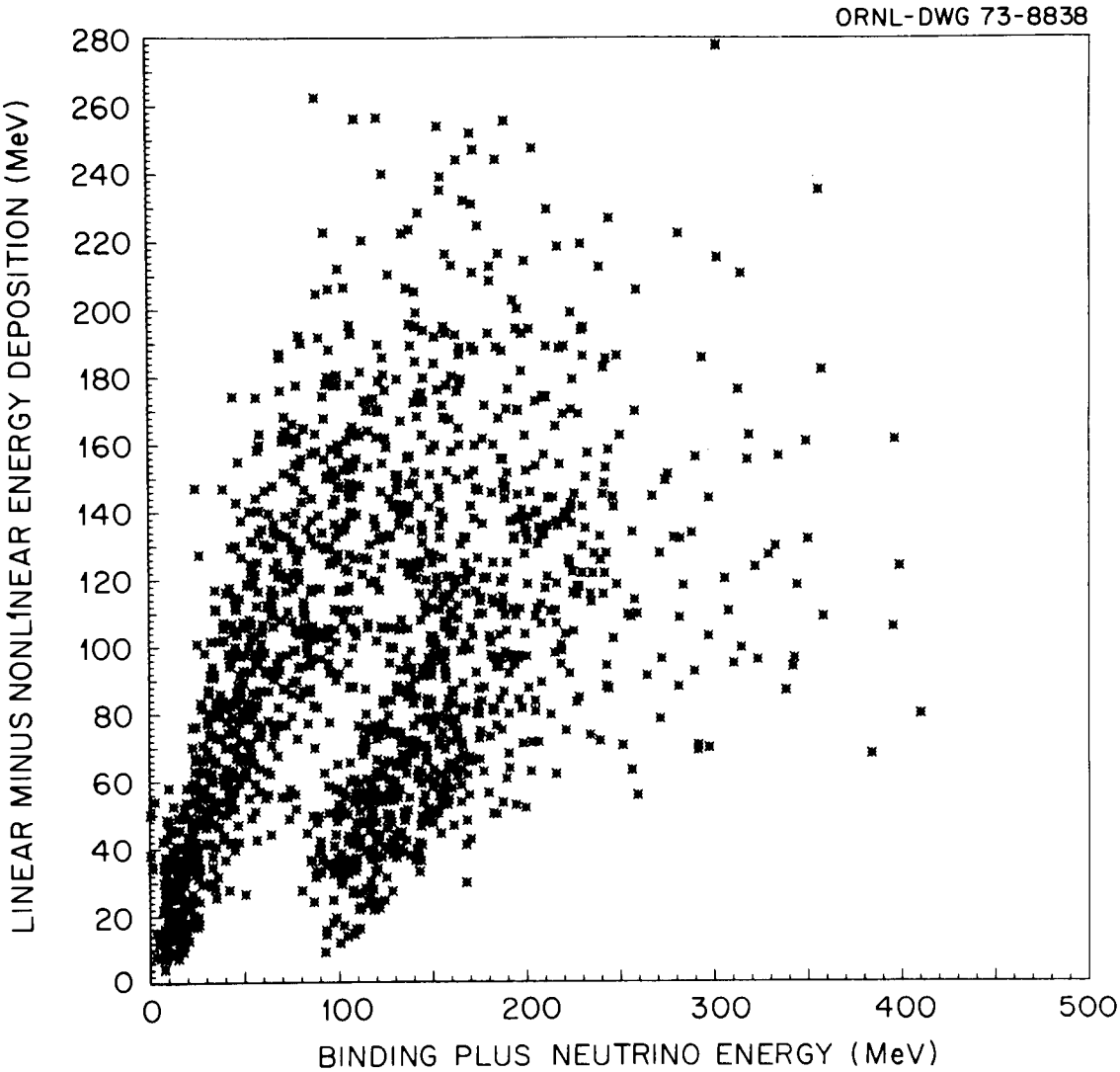

Fig. 8. Scatter plot of linear minus nonlinear energy deposition vs binding plus neutrino energy for incident 1-GeV/c π^+.

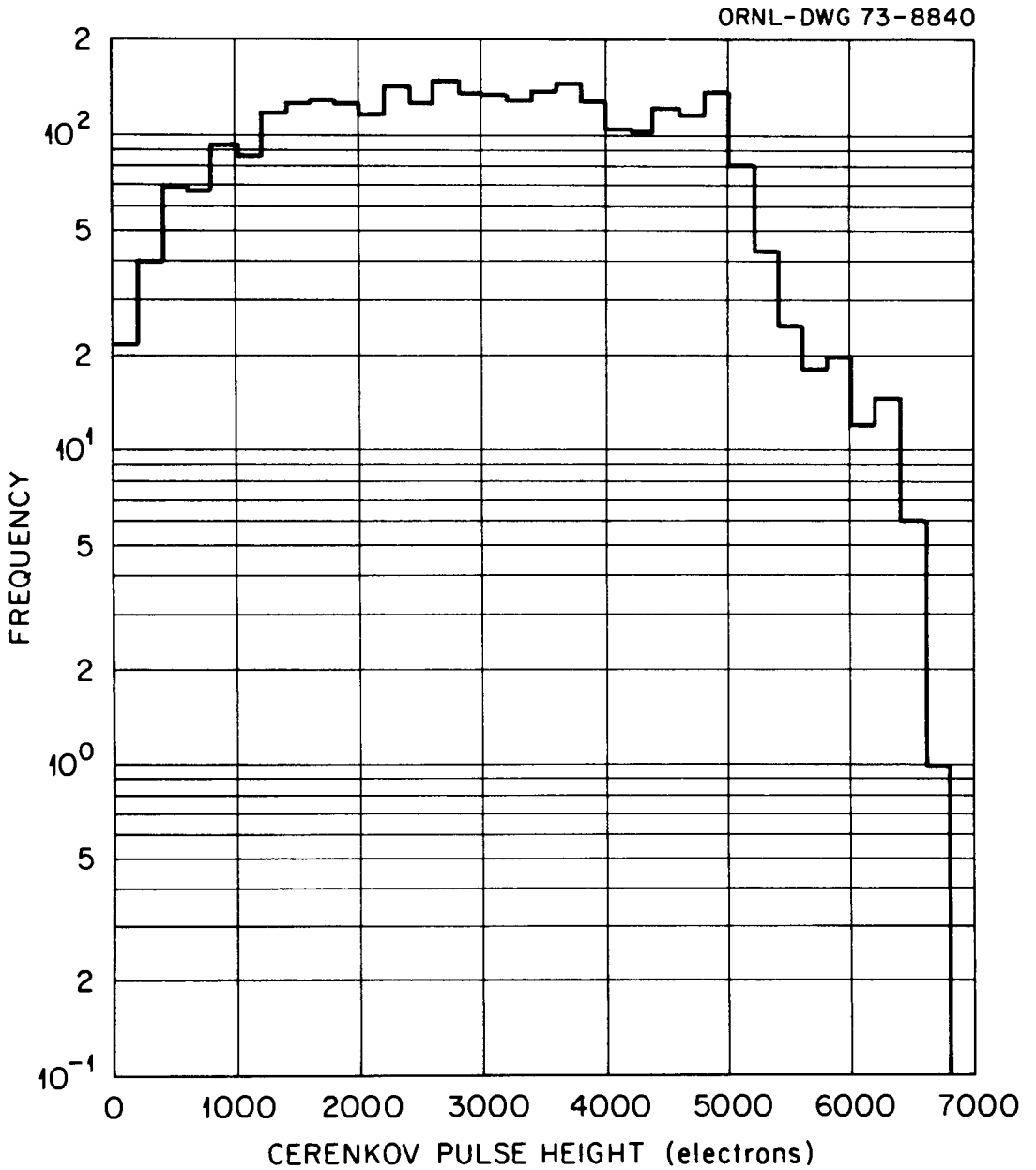

Fig. 9. Cerenkov pulse-height distribution for incident 1-GeV/c π^+.

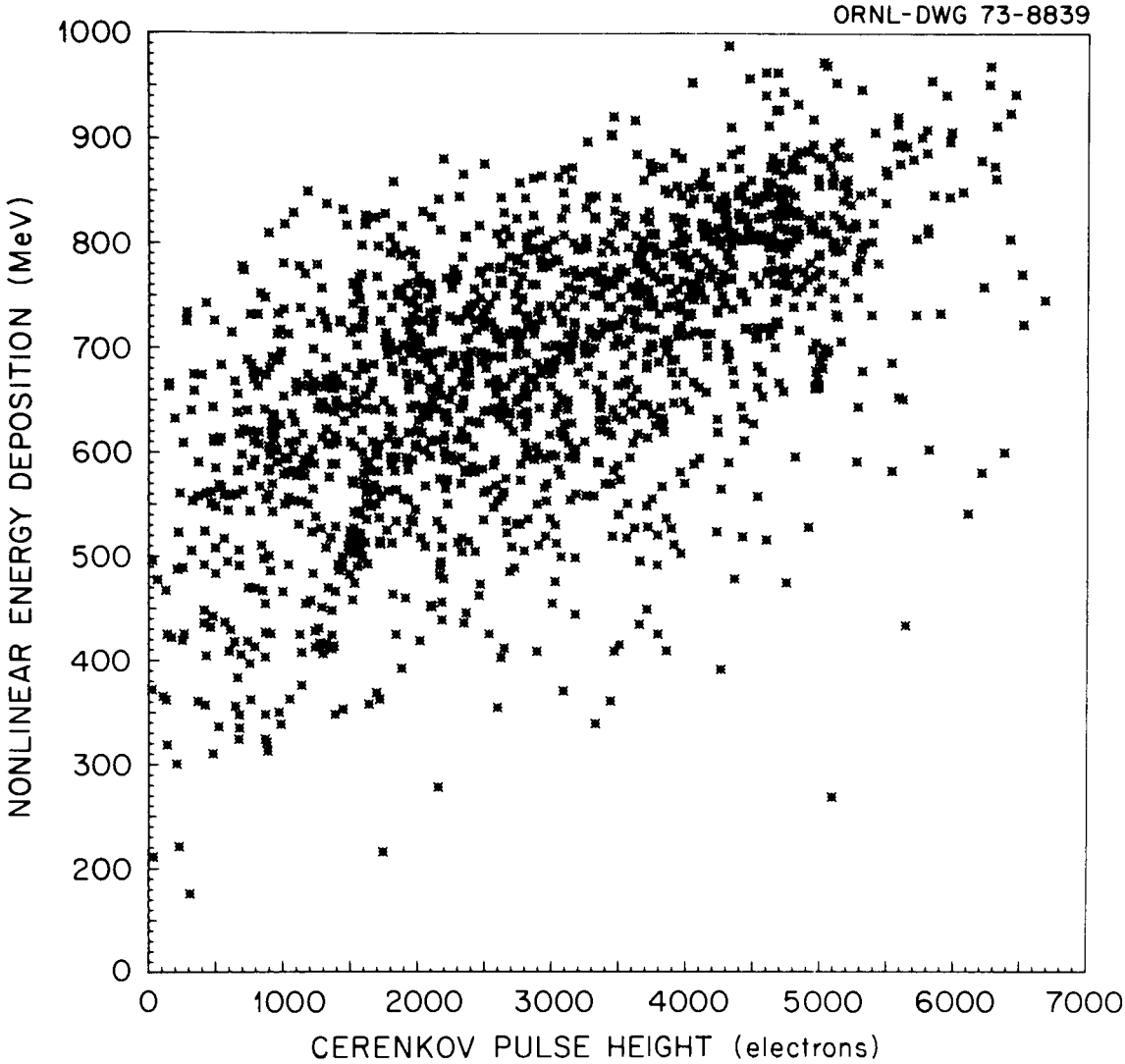

Fig. 10. Scatter plot of nonlinear energy deposition vs Cerenkov pulse height for incident 1-GeV/c π^+.

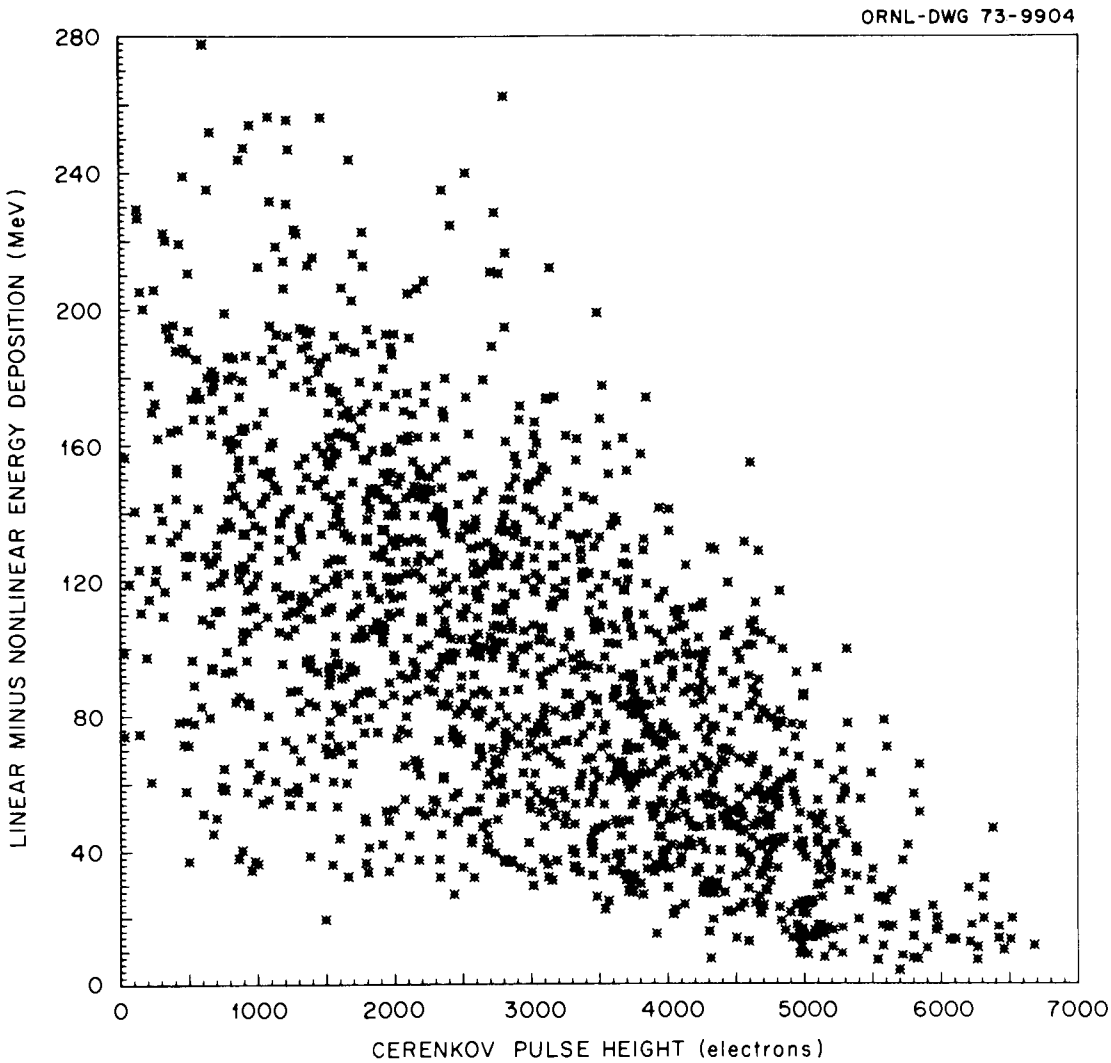

Fig. 11. Scatter plot of linear minus nonlinear energy deposition vs Cerenkov pulse height for incident 1-GeV/c π^+.

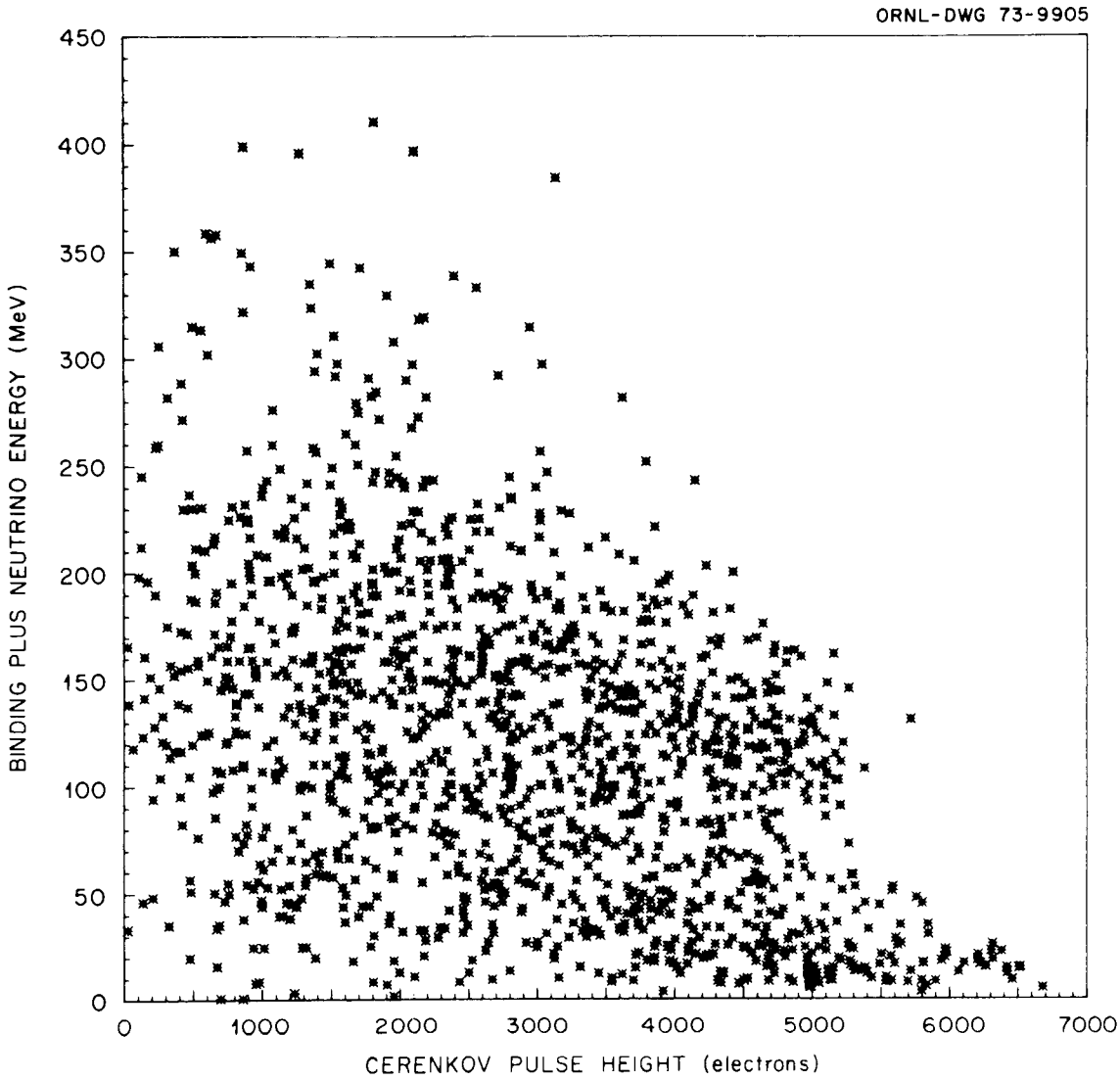

Fig. 12. Scatter plot of binding plus neutrino energy vs Cerenkov pulse height for incident 1-GeV/c π^+.

ORNL-DWG 73-8834

TABLE 1

SPATIAL ENERGY DEPOSITION IN A LARGE SCINTILLATION SPECTROMETER

TYPE OF INCIDENT PARTICLE PI +
MOMENTUM OF INCIDENT PARTICLE 1 GEV/C

ENERGY DEPOSITION
(MEV/CM**3)

DEPTH IN SPECTROMETER (CM)	RADIAL INTERVAL (CM) 0 TO 10	10 TO 20	20 TO 30	30 TO 40	40 TO 50	50 TO 60
0 TO 20	9.96E-03	3.82E-04	1.14E-04	4.98E-05	2.75E-05	1.73E-05
	1.4	4.3	4.1	7.1	6.2	7.7
20 TO 40	9.32E-03	6.78E-04	2.18E-04	8.24E-05	4.40E-05	2.51E-05
	1.3	3.4	3.0	4.5	5.3	6.8
40 TO 60	7.62E-03	7.11E-04	2.61E-04	1.09E-04	5.79E-05	3.42E-05
	1.7	2.2	4.2	5.6	5.9	7.5
60 TO 80	6.26E-03	7.28E-04	2.75E-04	1.35E-04	7.05E-05	4.38E-05
	2.2	3.7	4.0	5.1	3.5	3.8
80 TO 100	4.97E-03	6.23E-04	2.74E-04	1.44E-04	8.28E-05	4.21E-05
	2.0	4.1	4.2	5.0	4.0	5.0
100 TO 120	3.98E-03	4.79E-04	2.44E-04	1.34E-04	7.41E-05	4.37E-05
	2.3	4.8	3.7	2.9	3.0	6.1
120 TO 140	3.42E-03	3.72E-04	2.05E-04	1.12E-04	7.13E-05	4.76E-05
	2.5	4.6	3.2	4.8	6.5	6.6
140 TO 160	2.69E-03	3.22E-04	1.63E-04	9.06E-05	5.86E-05	4.46E-05
	3.5	6.2	4.6	4.6	5.2	7.1
160 TO 180	2.21E-03	2.20E-04	1.19E-04	8.02E-05	4.72E-05	3.67E-05
	3.0	5.1	7.7	7.8	7.6	5.2
180 TO 200	1.70E-03	1.64E-04	9.53E-05	5.77E-05	3.96E-05	3.28E-05
	2.3	5.7	7.0	8.2	5.2	6.5
200 TO 220	1.41E-03	1.35E-04	7.90E-05	5.64E-05	3.51E-05	2.61E-05
	3.9	6.4	7.7	7.9	9.5	5.0
220 TO 240	1.25E-03	1.06E-04	5.60E-05	4.28E-05	2.81E-05	2.48E-05
	3.0	8.1	8.9	8.9	7.6	9.3
240 TO 260	9.94E-04	7.31E-05	3.73E-05	3.02E-05	2.41E-05	1.93E-05
	4.3	12.8	7.2	5.2	9.6	11.4
260 TO 280	8.04E-04	8.52E-05	3.69E-05	2.82E-05	2.08E-05	1.41E-05
	5.3	10.3	5.4	10.5	9.5	12.1
280 TO 300	6.85E-04	6.66E-05	3.94E-05	2.36E-05	1.82E-05	1.62E-05
	7.9	8.5	11.5	9.0	8.0	13.5
300 TO 325	5.87E-04	6.02E-05	3.06E-05	2.36E-05	1.53E-05	1.14E-05
	6.8	9.7	8.7	9.6	13.1	9.4
325 TO 356	3.93E-04	4.65E-05	1.86E-05	1.10E-05	8.11E-06	5.54E-06
	9.0	9.5	21.7	17.4	18.9	13.5

ORNL-DWG 73-8835

TABLE 1 (CONT'D)

SPATIAL ENERGY DEPOSITION IN A LARGE SCINTILLATION SPECTROMETER

TYPE OF INCIDENT PARTICLE PI +
MOMENTUM OF INCIDENT PARTICLE 1 GEV/C

ENERGY DEPOSITION
(MEV/CM**3)

DEPTH IN SPECTROMETER (CM)	RADIAL INTERVAL (CM) 60 TO 70	70 TO 80	80 TO 90	90 TO 100	100 TO 110	110 TO 127
0 TO 20	1.11E-05	8.34E-06	5.05E-06	4.46E-06	3.84E-06	2.55E-06
	13.4	10.0	11.9	6.6	13.0	12.9
20 TO 40	1.56E-05	1.18E-05	8.39E-06	6.19E-06	5.00E-06	3.60E-06
	6.1	8.5	12.4	12.0	14.7	10.2
40 TO 60	2.40E-05	1.53E-05	1.08E-05	7.66E-06	6.13E-06	3.93E-06
	8.5	6.8	9.3	8.1	11.5	12.5
60 TO 80	3.06E-05	1.60E-05	1.06E-05	7.55E-06	6.28E-06	4.45E-06
	5.9	5.1	11.0	10.9	8.0	6.6
80 TO 100	2.69E-05	1.74E-05	1.29E-05	1.06E-05	6.24E-06	5.40E-06
	6.2	8.0	5.2	7.7	7.0	8.1
100 TO 120	2.75E-05	1.84E-05	1.49E-05	9.89E-06	7.35E-06	5.36E-06
	4.1	6.1	7.6	6.4	6.1	6.7
120 TO 140	3.10E-05	2.08E-05	1.45E-05	1.07E-05	6.93E-06	4.77E-06
	8.0	5.2	8.7	9.7	6.7	6.5
140 TO 160	3.05E-05	1.65E-05	9.95E-06	8.65E-06	7.02E-06	4.75E-06
	6.3	6.1	6.9	12.1	11.0	12.3
160 TO 180	2.55E-05	1.88E-05	1.29E-05	8.28E-06	6.78E-06	3.95E-06
	7.3	7.4	10.0	8.5	9.5	10.3
180 TO 200	2.41E-05	1.75E-05	1.16E-05	9.53E-06	5.96E-06	4.12E-06
	9.3	7.2	6.4	10.0	17.2	9.0
200 TO 220	1.93E-05	1.62E-05	1.24E-05	9.11E-06	8.78E-06	4.85E-06
	7.6	7.8	6.8	7.7	7.9	11.9
220 TO 240	1.63E-05	1.15E-05	9.06E-06	9.15E-06	6.48E-06	4.44E-06
	8.5	7.4	10.4	9.6	9.4	11.8
240 TO 260	1.63E-05	1.16E-05	8.25E-06	5.84E-06	4.28E-06	3.80E-06
	8.9	9.6	11.2	12.1	7.7	12.5
260 TO 280	1.16E-05	9.43E-06	6.70E-06	6.17E-06	4.49E-06	3.13E-06
	12.1	8.1	10.1	11.1	10.0	12.9
280 TO 300	8.34E-06	7.53E-06	5.47E-06	4.43E-06	3.66E-06	2.67E-06
	13.5	10.2	12.2	14.5	17.8	10.8
300 TO 325	7.01E-06	5.70E-06	5.33E-06	3.72E-06	2.67E-06	1.90E-06
	15.7	10.3	16.2	20.9	14.5	12.0
325 TO 356	4.04E-06	3.88E-06	2.41E-06	2.33E-06	2.23E-06	1.18E-06
	20.9	19.7	13.9	16.3	15.5	15.3

Table 2

Energy Deposition and Leakage Produced by the Interaction of 1-GeV/c π^+ in a Large Scintillation Spectrometer[a]

Energy Deposition (MeV)	Linear	Nonlinear[b]
Primary ionization	170.	166.
Secondary proton ionization	265.	213.
Secondary $\pi^\pm$ ionization	127.	123.
Secondary $\mu^\pm$ ionization	15.5	14.9
Nuclear recoil and evaporated charged particles other than protons[c]	29.4	4.70
Excitation energy following evaporation[c]	6.76	6.76
Neutrons with energy < 15 MeV[c]	15.9	6.81
Electromagnetic from the decay of π°'s	134.	134.
Electromagnetic from the decay of $\mu^\pm$'s	16.1	16.1
Total Deposition	780.	686.

Leakage Energy (MeV)	Front	Side	Back
p	0.86	0.78	0.46
n	4.52	17.9	4.43
$\pi^\pm$ [d]	8.43	6.97	6.26
$\mu^\pm$ [d]	0.16	0.85	3.05
γ	12.6	32.2	4.20
$e^\pm$ [d]	2.63	5.97	1.22
Total	29.2	64.7	19.6

Total Leakage = 114. MeV

(Binding energy + ν energy) = 117. MeV

Electromagnetic Source Energy = 208. MeV

a. CH_2, ρ = 0.87 g/cm^3; 254 cm in diameter, 355.6 cm in length.
b. kB = 0.01 (g/cm^2)/MeV.
c. Assumed to deposit their energy at their point of origin.
d. Includes rest mass energy.

Table 3

Average Cerenkov Pulse Height From the Interaction of 1-GeV/c Incident π^+ in a Large Spectrometer

	Cerenkov Pulse Height (electrons)
Primary particles	1289.
Secondary protons	12.6
Secondary charged pions	633.
Secondary muons	82.9
Electromagnetic cascade	944.
Total	2961.

Because of the nonlinearity of this device with respect to light output vs energy deposition, not all of the deposited energy can be viewed due to saturation. The column in table 2 labeled "nonlinear" gives the amount of energy deposited which, according to our light curve normalization (see sec. 2), can be viewed. The electromagnetic contribution is unaffected by the saturation effect, whereas the heavy-recoil and evaporation fragments show the largest deviation.

All of the quantities shown in table 2, i.e., binding energy plus neutrino energy, the leakage energy, and the saturation effect, have a direct bearing on the resolution of this spectrometer. The calculated resolution of this device for 1-GeV/c π^+ can be seen in the pulse-height distribution given in fig. 5. (All pulse-height distributions are normalized to 5000 events, except for fig. 9 which has 3000 events.) The solid histogram represents the pulse-height distribution obtained with the linear data, i.e., with the saturation effect neglected. The dashed histogram represents the pulse-height distribution with the effect of saturation taken into consideration. It is clear from this figure that the saturation effect is not small and should be taken into account. The resolution obtained (for the dashed histogram) considering the full width at half maximum is 40% (+ 16%, - 24%).

Since no time gate has been applied to these calculations (and most scintillation time gates are set at ~ 50 nsec), the amount of light viewed experimentally should be slightly less than that shown in fig. 5. One of the many reasons for this originates from positrons which are born from the decay of positively charged muons which come from positively charged pions decaying at rest. The number of positively charged pions decaying at

rest per incident 1-GeV/c π^+ was calculated to be 0.44 ± 0.03. Not only is a lot of energy lost to neutrinos but, experimentally, the energy deposition of the positron (~ 40 MeV) will not be detected.

In order to obtain a more complete understanding of this particular spectrometer, several scatter plots (all scatter plots contain 1500 events) are given in figs. 6, 7, and 8. The binding energy plus neutrino energy is shown in fig. 6 as a function of linear energy deposition. The line of points on the right side of the figure is the energy conservation line; i.e., the sum of energy deposition plus binding and neutrino energy gives the total energy of the incident 1-GeV/c π^+. Any point to the left of this line indicates the degree of leakage energy.

The difference between the linear- and nonlinear-energy deposition vs the linear energy deposition is shown in fig. 7. The difference between the linear- and nonlinear-energy deposition vs the binding plus neutrino energy is shown in fig. 8. The data in this figure split into two distinct groups. The group which appears to intersect the x axis at ~ 100 MeV is due to secondary positively charged pions which slow down to rest. As stated before, a significant amount of neutrino energy (~ 100 MeV) is lost when this occurs.

Since a combination of scintillating and Cerenkov-response devices is employed in many experiments, the expected Cerenkov pulse-height distribution for the spectrometer is given in fig. 9, and the average individual contributors are given in table 3. Even though this represents an unrealistic case since it is next to impossible to separate the scintillation and Cerenkov pulse in the same material, many of the conclusions which can be drawn are still applicable.

In contrast to the scintillation pulse-height distribution (fig. 5), the Cerenkov response is relatively flat and would be of little use at this

energy for determining the energy of incident particles. The small peak at 4900 electrons primarily results from the few incident particles which completely transverse the device without interacting. The average contributions to the pulse-height distribution are given in table 3. Since protons have a relatively high threshold for producing Cerenkov light ($\sim$ 340 MeV), it is not unexpected that the secondary proton contribution should be small relative to the pion, muon, electron, and positron contributions.

The one-to-one correlation between the scintillation (nonlinear) and Cerenkov pulses is given in fig. 10 in terms of a scatter plot. As can be seen, a large Cerenkov response usually necessitates a large scintillation response and vice versa. This is the expected result since a large scintillation response usually requires a large electromagnetic cascade which also leads to a large Cerenkov response.

The one-to-one correlation between the linear minus nonlinear scintillation pulses and the Cerenkov pulse is shown in fig. 11, and the correlation between the binding energy plus neutrino energy and Cerenkov pulse is shown in fig. 12. As the difference between the linear and nonlinear pulses approaches zero indicating a large electromagnetic contribution, the Cerenkov response becomes large. As the binding energy plus neutrino energy becomes large indicating that less energy is available for the electromagnetic cascade, the Cerenkov pulse becomes small. These correlations do not indicate anything surprizingly new, but they do indicate the amount of spread in the correlations that can be expected.

Since much of the previous discussion concerning the incident 1-GeV/c π^+ is applicable to the remaining cases, only a brief summary of each case will be presented.

The spatial distribution for 1-GeV/c incident π^- is given in table 4, and the spatially integrated individual contributions and the leakage energy are given in table 5. The total containment for this case is slightly less than that for the 1-GeV/c π^+ case. This decrease in containment is due primarily to the availability of one reaction channel open to the π^- but not to the π^+, i.e., $\pi^- + p \rightarrow 2\pi^\circ + n$. This reaction channel allows for more neutron and gamma-ray leakage. The pulse-height distributions are given in fig. 13, and a comparison between the 1-GeV/c π^+ and π^- nonlinear pulse-height distributions is given in fig. 14. The binding plus neutrino energy vs energy deposition (linear), the linear-nonlinear energy deposition vs energy deposition (linear), and the linear-nonlinear energy deposition vs binding plus neutrino energy are shown in figs. 15-17, respectively. The data in fig. 17 do not split distinctly into two groups as did the data for the incident 1-GeV/c π^+, indicating a large decrease in the number of secondary positively charged pions which come to rest.

Similar data for 3-GeV/c incident π^- are given in tables 6 and 7 and in figs. 18-21. The large peak at approximately 700 MeV in fig. 18 is due to those few incident particles which transverse the entire device without interacting. Due to the increase in leakage at this energy, the energy conservation line, so evident in fig. 6, is not nearly as evident in fig. 19.

The data for 1-GeV/c incident protons are given in table 8 and in fig. 22. The spatial dependence of the energy deposition is not given for this case since many of these incident particles will slow down due to ionization and excitation rather than undergo nuclear interaction. Those primary protons that do interact usually elastically scatter with the hydrogen in the media, thereby enhancing the probability of slowing down rather than undergoing

TABLE 4

SPATIAL ENERGY DEPOSITION IN A LARGE SCINTILLATION SPECTROMETER

TYPE OF INCIDENT PARTICLE PI -
MOMENTUM OF INCIDENT PARTICLE 1 GEV/C

ENERGY DEPOSITION
(MEV/CM**3)

DEPTH IN SPECTROMETER (CM)	RADIAL INTERVAL (CM) 0 TO 10	10 TO 20	20 TO 30	30 TO 40	40 TO 50	50 TO 60
0 TO 20	9.16E-03	3.68E-04	1.23E-04	6.76E-05	3.59E-05	2.26E-05
	1.6	4.6	6.3	5.8	5.7	7.9
20 TO 40	8.67E-03	6.69E-04	2.32E-04	1.05E-04	5.79E-05	3.60E-05
	1.2	2.9	2.8	5.3	4.0	2.9
40 TO 60	7.02E-03	8.19E-04	2.97E-04	1.38E-04	7.08E-05	3.97E-05
	1.5	4.8	4.9	4.4	5.3	6.6
60 TO 80	5.18E-03	7.52E-04	3.09E-04	1.54E-04	7.94E-05	4.73E-05
	1.2	3.3	5.3	5.0	3.6	3.6
80 TO 100	4.36E-03	5.89E-04	2.88E-04	1.46E-04	8.17E-05	5.21E-05
	1.7	2.3	4.1	3.0	4.7	8.7
100 TO 120	3.42E-03	4.62E-04	2.45E-04	1.36E-04	9.01E-05	5.03E-05
	3.5	3.0	4.0	4.8	5.9	4.0
120 TO 140	2.76E-03	3.55E-04	1.90E-04	1.22E-04	7.89E-05	5.55E-05
	3.5	4.5	3.3	4.7	5.9	5.2
140 TO 160	2.09E-03	2.73E-04	1.50E-04	9.75E-05	7.00E-05	4.31E-05
	4.2	4.2	3.7	4.5	4.2	6.5
160 TO 180	1.63E-03	2.29E-04	1.27E-04	8.51E-05	5.31E-05	3.83E-05
	4.1	5.7	6.5	5.7	6.1	4.8
180 TO 200	1.27E-03	1.49E-04	9.76E-05	6.52E-05	4.84E-05	3.38E-05
	3.6	7.3	6.5	6.3	8.9	6.3
200 TO 220	1.08E-03	1.25E-04	7.17E-05	4.79E-05	3.86E-05	2.44E-05
	4.2	7.5	8.0	8.9	9.3	8.5
220 TO 240	8.89E-04	8.74E-05	6.37E-05	3.83E-05	3.10E-05	2.30E-05
	5.7	8.4	8.1	10.1	12.1	8.3
240 TO 260	7.11E-04	7.70E-05	5.04E-05	3.37E-05	2.47E-05	1.96E-05
	5.8	8.0	9.3	7.9	5.7	7.6
260 TO 280	5.51E-04	5.46E-05	3.56E-05	3.26E-05	2.41E-05	1.69E-05
	6.1	13.9	6.2	7.9	10.3	9.9
280 TO 300	4.55E-04	4.63E-05	2.68E-05	2.48E-05	1.91E-05	1.56E-05
	6.8	12.3	15.2	11.8	9.0	13.9
300 TO 325	3.10E-04	4.41E-05	2.32E-05	1.77E-05	1.71E-05	1.31E-05
	6.8	12.0	15.3	11.9	10.6	14.0
325 TO 356	2.16E-04	3.15E-05	1.49E-05	1.07E-05	8.98E-06	6.28E-06
	7.7	10.6	14.6	12.8	10.8	12.0

TABLE 4 (CONT'D)

SPATIAL ENERGY DEPOSITION IN A LARGE SCINTILLATION SPECTROMETER

TYPE OF INCIDENT PARTICLE PI -
MOMENTUM OF INCIDENT PARTICLE 1 GEV/C

ENERGY DEPOSITION
(MEV/CM**3)

DEPTH IN SPECTROMETER (CM)	RADIAL INTERVAL (CM) 60 TO 70	70 TO 80	80 TO 90	90 TO 100	100 TO 110	110 TO 127
0 TO 20	1.44E-05	1.09E-05	7.77E-06	6.21E-06	5.00E-06	3.65E-06
	5.8	7.1	7.6	6.6	7.8	9.3
20 TO 40	2.34E-05	1.77E-05	1.14E-05	7.71E-06	5.11E-06	3.81E-06
	9.0	7.9	7.3	7.0	14.4	10.2
40 TO 60	2.81E-05	1.81E-05	1.27E-05	9.12E-06	5.95E-06	4.84E-06
	6.4	6.1	7.3	9.7	12.0	8.7
60 TO 80	3.25E-05	2.06E-05	1.56E-05	1.16E-05	8.10E-06	6.27E-06
	5.3	8.0	5.8	13.8	10.5	7.9
80 TO 100	3.55E-05	2.44E-05	1.62E-05	1.12E-05	8.13E-06	5.20E-06
	5.9	7.7	6.6	7.5	9.2	5.3
100 TO 120	3.27E-05	2.01E-05	1.66E-05	1.21E-05	9.10E-06	5.80E-06
	8.7	7.3	7.3	9.5	9.8	8.8
120 TO 140	3.51E-05	2.37E-05	1.39E-05	1.06E-05	9.01E-06	5.69E-06
	8.4	6.4	6.0	11.1	4.7	7.7
140 TO 160	3.15E-05	2.21E-05	1.62E-05	1.13E-05	9.12E-06	6.49E-06
	4.3	5.4	8.1	9.0	7.2	9.2
160 TO 180	2.57E-05	2.17E-05	1.65E-05	1.02E-05	8.83E-06	6.54E-06
	6.8	4.5	4.3	5.9	6.7	8.5
180 TO 200	2.46E-05	2.12E-05	1.37E-05	8.16E-06	7.37E-06	5.20E-06
	7.6	7.4	8.6	11.4	6.5	7.1
200 TO 220	1.64E-05	1.43E-05	1.27E-05	1.02E-05	6.83E-06	4.52E-06
	7.4	11.8	8.4	3.7	8.5	7.6
220 TO 240	1.68E-05	1.33E-05	1.05E-05	8.79E-06	6.26E-06	5.17E-06
	8.7	9.7	13.7	11.3	9.7	4.3
240 TO 260	1.46E-05	1.09E-05	9.14E-06	8.26E-06	6.15E-06	4.84E-06
	9.1	13.6	11.7	16.3	11.0	7.1
260 TO 280	1.40E-05	1.00E-05	7.56E-06	6.53E-06	6.14E-06	3.78E-06
	10.7	9.8	9.6	14.7	15.4	10.5
280 TO 300	1.05E-05	7.72E-06	6.17E-06	5.09E-06	3.83E-06	3.02E-06
	13.5	8.6	12.6	12.3	14.4	10.6
300 TO 325	8.95E-06	6.90E-06	5.60E-06	2.89E-06	2.97E-06	2.46E-06
	16.1	9.3	9.8	12.8	14.1	12.3
325 TO 356	5.04E-06	4.51E-06	4.44E-06	3.87E-06	3.02E-06	2.04E-06
	12.0	13.0	12.3	14.7	10.7	19.4

Table 5

Energy Deposition and Leakage Produced by the Interaction of 1-GeV/c π^- in a Large Scintillation Spectrometer[a]

Energy Deposition (MeV)	Linear	Nonlinear[b]
Primary ionization	147.	144.
Secondary proton ionization	240.	188.
Secondary $\pi^\pm$ ionization	131.	127.
Secondary $\mu^\pm$ ionization	13.4	12.9
Nuclear recoil and evaporated charged particles other than protons[c]	39.3	5.71
Excitation energy following evaporation[c]	9.26	9.26
Neutrons with energy < 15 MeV[c]	26.4	11.4
Electromagnetic from the decay of π°'s	146.	146.
Electromagnetic from the decay of $\mu^\pm$'s	7.05	7.05
Total Deposition	760.	651.

Leakage Energy (MeV)	Front	Side	Back
p	0.35	0.92	0.30
n	8.21	33.8	8.88
$\pi^\pm$ d	11.1	5.87	5.05
$\mu^\pm$ d	0.15	0.77	2.49
γ	15.8	36.4	6.69
$e^\pm$ d	1.75	7.17	1.02
Total	37.4	85.0	24.4

Total Leakage = 147. MeV

(Binding energy + ν energy) = 104. MeV

Electromagnetic Source Energy = 222. MeV

a. CH_2, ρ = 0.87 g/cm^3; 254 cm in diameter, 355.6 cm in length.
b. kB = 0.01 (g/cm^2)/MeV.
c. Assumed to deposit their energy at their point of origin.
d. Includes rest mass energy.

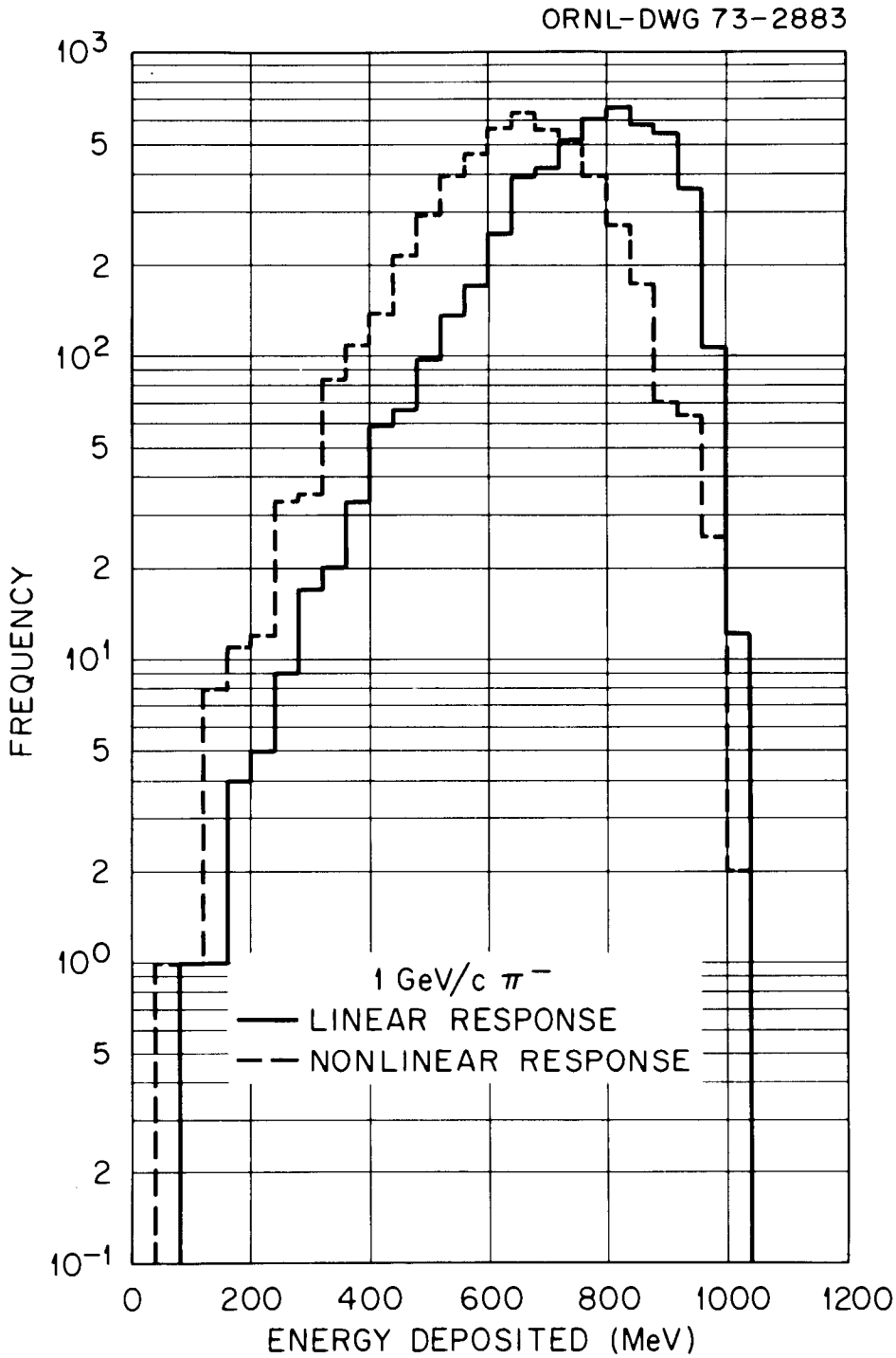

Fig. 13. Linear and nonlinear scintillation pulse-height distributions for incident 1-GeV/c π^-.

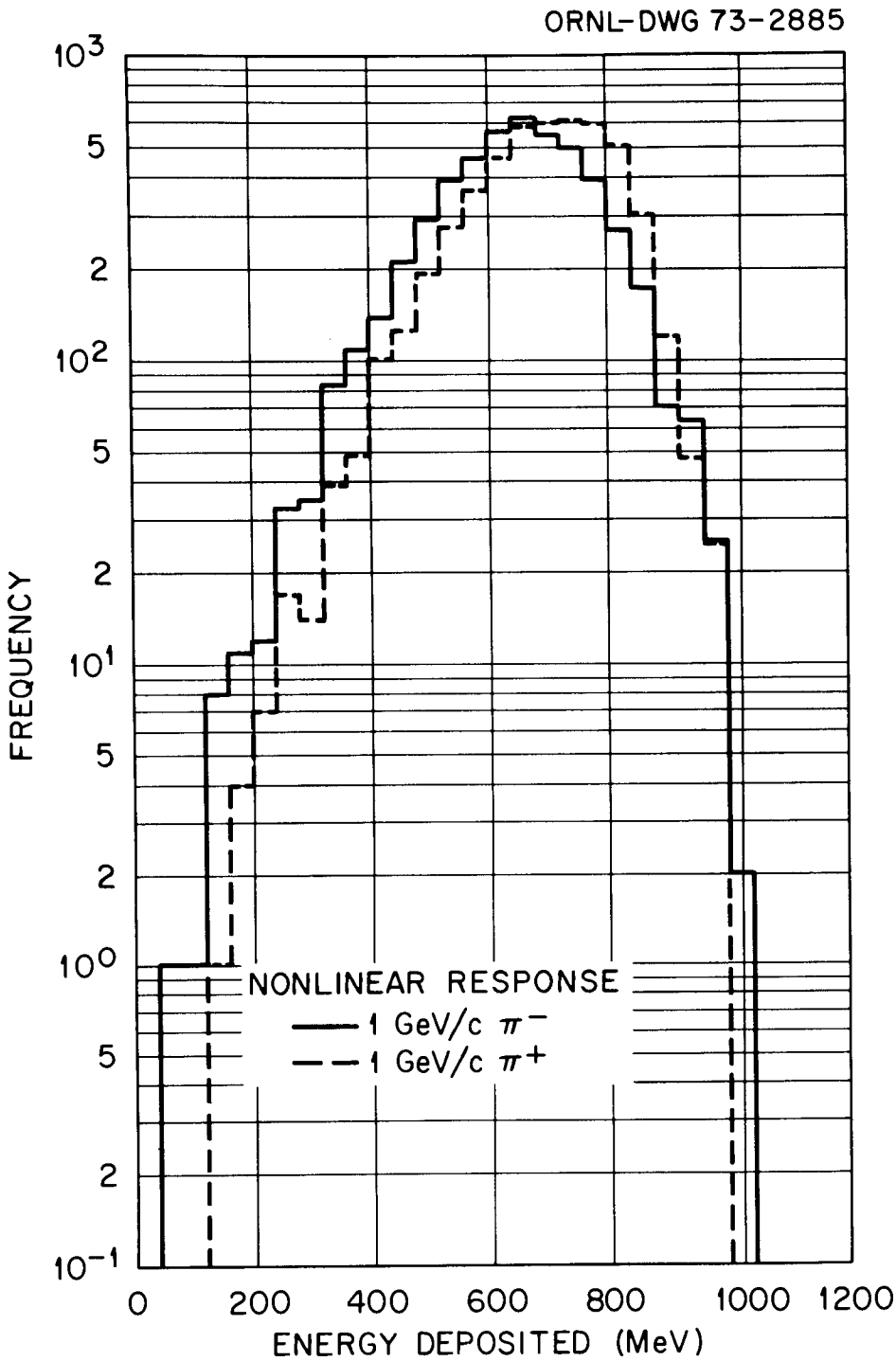

Fig. 14. Comparison between the nonlinear scintillation pulse-height distributions for incident 1-GeV/c π^+ and 1-GeV/c π^-.

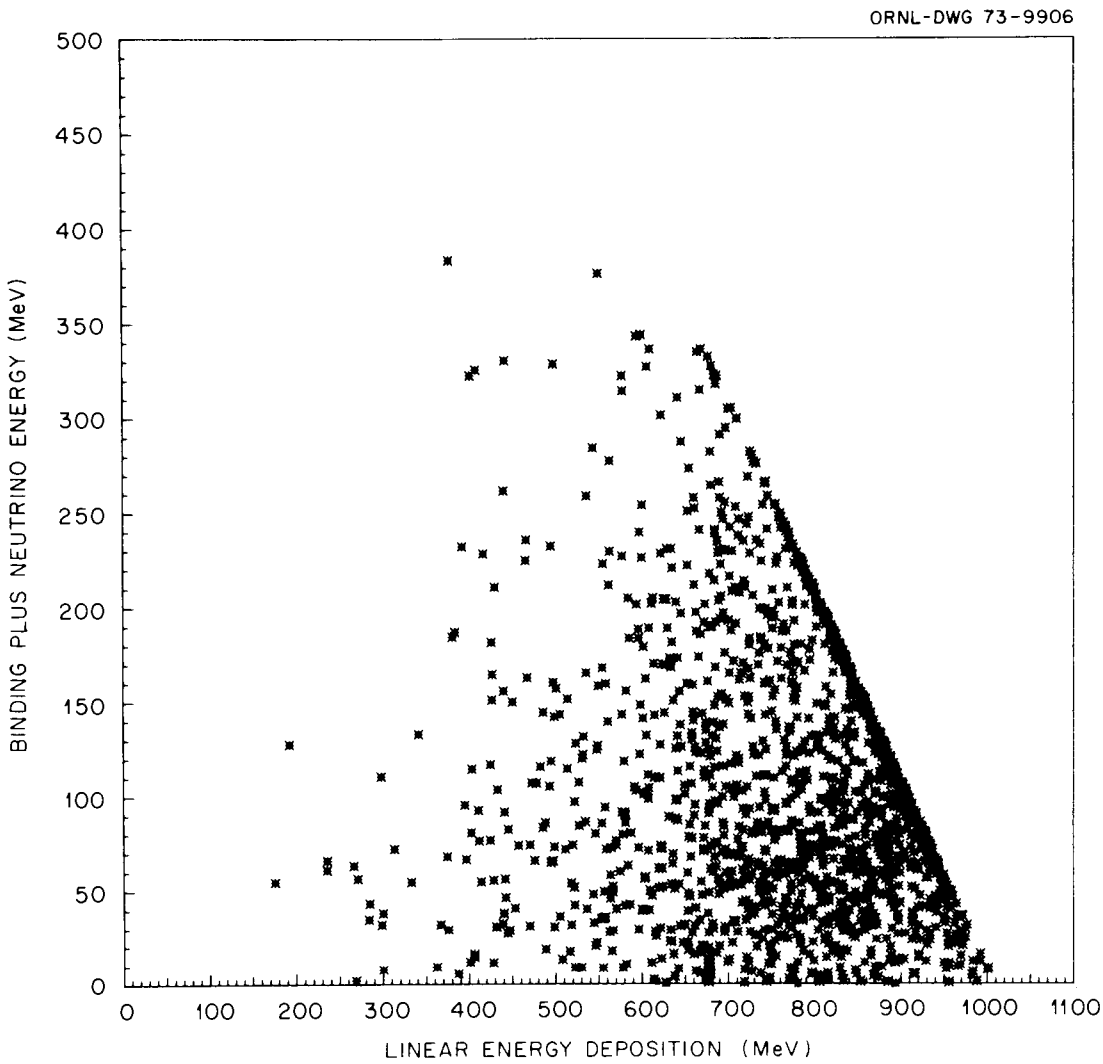

Fig. 15. Scatter plot of binding plus neutrino energy vs linear energy deposition for incident 1-GeV/c π^-.

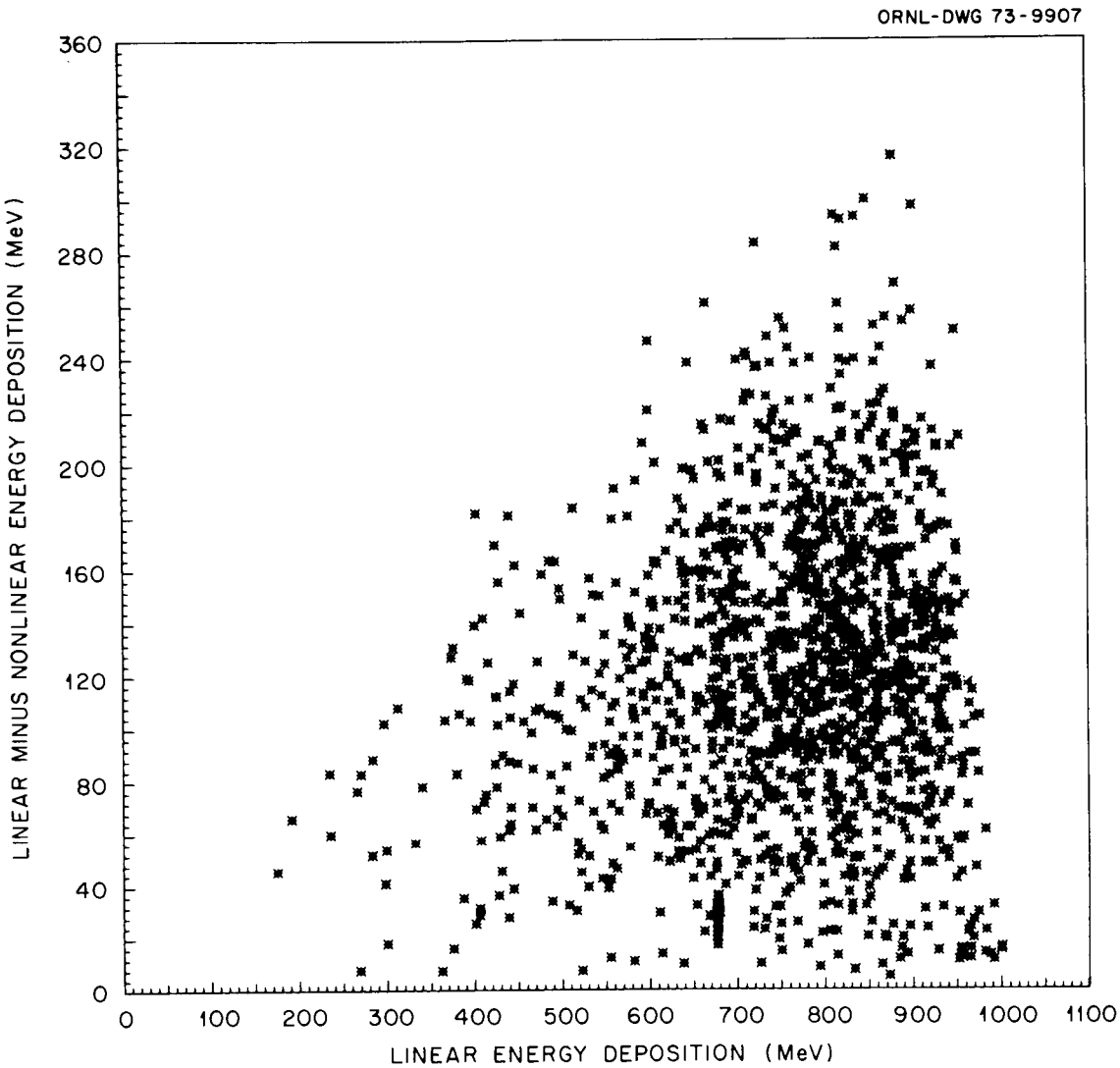

Fig. 16. Scatter plot of linear minus nonlinear energy deposition vs linear energy deposition for incident 1-GeV/c π^-.

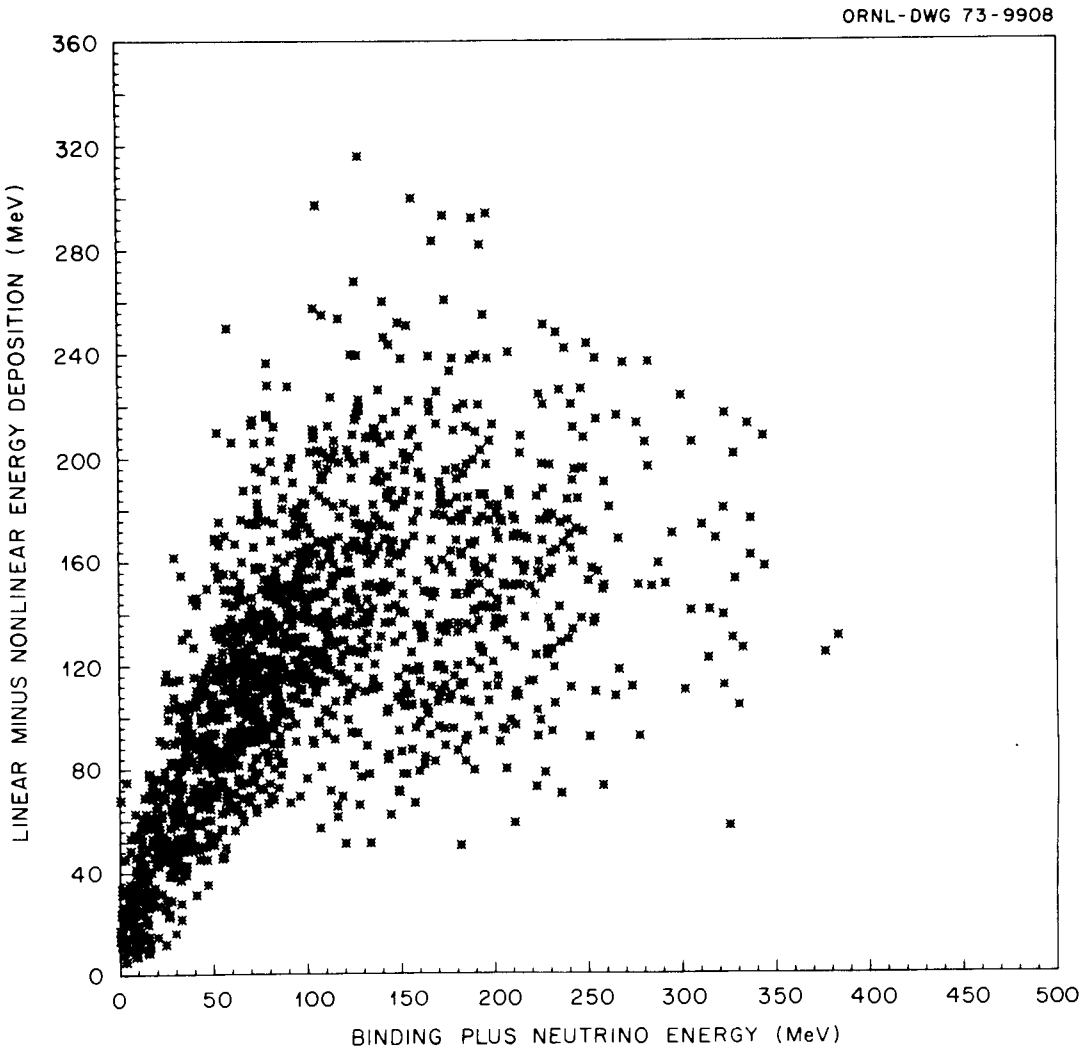

Fig. 17. Scatter plot of linear minus nonlinear energy deposition vs binding plus neutrino energy for incident 1-GeV/c π^-.

TABLE 6

SPATIAL ENERGY DEPOSITION IN A LARGE SCINTILLATION SPECTROMETER

TYPE OF INCIDENT PARTICLE PI -
MOMENTUM OF INCIDENT PARTICLE 3 GEV/C

ENERGY DEPOSITION
(MEV/CM**3)

DEPTH IN SPECTROMETER (CM)	RADIAL INTERVAL (CM) 0 TO 10	10 TO 20	20 TO 30	30 TO 40	40 TO 50	50 TO 60
0 TO 20	1.01E-02	3.66E-04	1.22E-04	5.86E-05	4.21E-05	2.72E-05
	1.2	5.1	7.5	6.6	5.4	10.0
20 TO 40	1.08E-02	9.08E-04	2.89E-04	1.31E-04	7.01E-05	4.23E-05
	1.3	5.0	4.5	5.8	6.2	4.1
40 TO 60	9.55E-03	1.18E-03	4.97E-04	2.27E-04	1.14E-04	6.00E-05
	1.9	4.7	5.4	5.4	7.4	4.1
60 TO 80	8.39E-03	1.41E-03	6.00E-04	3.05E-04	1.69E-04	9.80E-05
	2.4	5.1	4.7	5.9	5.6	5.9
80 TO 100	7.22E-03	1.46E-03	6.90E-04	3.85E-04	2.21E-04	1.35E-04
	1.5	6.6	1.7	7.7	7.6	5.3
100 TO 120	6.41E-03	1.30E-03	7.03E-04	4.03E-04	2.42E-04	1.59E-04
	2.2	4.6	4.2	4.7	3.7	6.0
120 TO 140	5.26E-03	1.25E-03	6.62E-04	4.20E-04	2.59E-04	1.55E-04
	2.6	2.6	3.1	4.9	2.1	2.2
140 TO 160	4.35E-03	1.08E-03	5.68E-04	4.16E-04	2.68E-04	1.83E-04
	5.5	4.3	5.6	2.5	6.1	4.8
160 TO 180	3.71E-03	9.72E-04	5.65E-04	3.46E-04	2.39E-04	1.93E-04
	3.3	2.9	2.4	4.9	6.2	6.5
180 TO 200	3.00E-03	8.16E-04	4.96E-04	3.06E-04	2.21E-04	1.72E-04
	5.8	4.1	4.4	7.1	5.1	5.0
200 TO 220	2.44E-03	6.28E-04	4.48E-04	2.99E-04	2.03E-04	1.43E-04
	2.0	3.2	2.1	6.6	8.0	6.3
220 TO 240	2.17E-03	5.81E-04	3.47E-04	2.55E-04	1.86E-04	1.41E-04
	5.7	7.9	10.1	6.1	7.4	9.3
240 TO 260	1.81E-03	5.12E-04	3.23E-04	2.30E-04	1.54E-04	1.25E-04
	6.3	9.2	8.9	5.9	5.4	7.1
260 TO 280	1.50E-03	4.67E-04	2.65E-04	1.80E-04	1.31E-04	1.08E-04
	11.1	6.5	5.0	9.2	6.2	7.6
280 TO 300	1.08E-03	3.66E-04	2.41E-04	1.80E-04	1.35E-04	9.79E-05
	9.2	6.6	4.0	4.5	4.5	2.8
300 TO 325	9.08E-04	3.08E-04	1.99E-04	1.63E-04	1.19E-04	8.32E-05
	11.0	8.1	5.8	3.9	6.0	11.1
325 TO 356	6.35E-04	2.15E-04	1.52E-04	1.13E-04	8.82E-05	6.94E-05
	13.7	4.5	8.9	6.4	4.3	7.1

TABLE 6 (CONT'D)

SPATIAL ENERGY DEPOSITION IN A LARGE SCINTILLATION SPECTROMETER

TYPE OF INCIDENT PARTICLE PI -
MOMENTUM OF INCIDENT PARTICLE 3 GEV/C

ENERGY DEPOSITION
(MEV/CM**3)

DEPTH IN SPECTROMETER (CM)	RADIAL INTERVAL (CM) 60 TO 70	70 TO 80	80 TO 90	90 TO 100	100 TO 110	110 TO 127
0 TO 20	1.71E-05	1.32E-05	8.57E-06	5.69E-06	5.53E-06	3.93E-06
	12.9	10.0	17.7	13.6	15.4	15.9
20 TO 40	2.63E-05	1.59E-05	1.20E-05	1.19E-05	8.24E-06	5.72E-06
	10.2	7.7	8.5	16.0	19.5	15.9
40 TO 60	3.69E-05	2.46E-05	1.64E-05	1.25E-05	8.42E-06	6.42E-06
	3.2	9.7	13.4	6.2	4.7	10.7
60 TO 80	5.69E-05	4.02E-05	2.60E-05	1.82E-05	1.27E-05	9.02E-06
	8.8	7.1	8.2	9.5	12.0	9.7
80 TO 100	8.27E-05	5.19E-05	3.38E-05	2.77E-05	1.84E-05	1.13E-05
	4.6	3.6	6.0	3.4	7.3	7.8
100 TO 120	9.67E-05	6.99E-05	5.41E-05	2.99E-05	2.01E-05	1.37E-05
	8.0	6.5	3.6	3.8	8.5	5.0
120 TO 140	1.23E-04	8.46E-05	5.12E-05	3.96E-05	2.87E-05	1.75E-05
	7.2	5.5	6.8	7.8	7.8	5.4
140 TO 160	1.18E-04	9.02E-05	6.12E-05	4.44E-05	3.18E-05	2.04E-05
	4.0	3.1	7.2	5.4	4.0	6.2
160 TO 180	1.26E-04	8.86E-05	6.46E-05	4.67E-05	3.53E-05	2.28E-05
	5.2	4.7	4.3	7.0	6.9	5.3
180 TO 200	1.24E-04	8.63E-05	6.49E-05	4.98E-05	3.76E-05	2.27E-05
	8.2	5.7	7.0	7.9	7.6	6.3
200 TO 220	1.15E-04	7.88E-05	6.04E-05	4.69E-05	3.78E-05	2.41E-05
	4.3	7.5	3.6	5.0	8.2	5.1
220 TO 240	1.00E-04	7.89E-05	5.72E-05	4.33E-05	3.56E-05	2.43E-05
	4.2	6.5	3.7	5.4	5.2	6.8
240 TO 260	9.39E-05	7.25E-05	5.35E-05	3.95E-05	3.12E-05	2.32E-05
	10.4	5.6	9.3	8.3	6.3	5.2
260 TO 280	7.76E-05	7.24E-05	5.06E-05	3.72E-05	3.01E-05	1.93E-05
	9.5	10.2	6.0	9.7	7.1	4.7
280 TO 300	8.19E-05	5.56E-05	4.50E-05	3.34E-05	2.72E-05	2.26E-05
	6.3	11.3	6.5	4.7	7.5	5.5
300 TO 325	6.75E-05	4.79E-05	3.88E-05	3.09E-05	2.27E-05	1.91E-05
	9.0	4.0	6.8	4.4	4.9	7.4
325 TO 356	5.31E-05	3.96E-05	3.06E-05	2.59E-05	1.95E-05	1.61E-05
	5.9	4.0	7.8	4.4	5.8	7.3

Table 7

Energy Deposition and Leakage Produced by the Interaction of 3-GeV/c π^- in a Large Scintillation Spectrometer[a]

Energy Deposition (MeV)	Linear	Nonlinear[b]
Primary ionization	184.	180.
Secondary proton ionization	657.	536.
Secondary $\pi^\pm$ ionization	330.	320.
Secondary $\mu^\pm$ ionization	14.3	13.7
Nuclear recoil and evaporated charged particles other than protons[c]	82.3	12.4
Excitation energy following evaporation[c]	19.1	19.1
Neutrons with energy < 15 MeV[c]	51.4	22.1
Electromagnetic from the decay of π°'s	638.	638.
Electromagnetic from the decay of $\mu^\pm$'s	15.7	15.7
Total Deposition	1991.	1757.

Leakage Energy (MeV)	Front	Side	Back
p	0.62	18.3	33.7
n	10.5	118.	88.6
$\pi^\pm$ [d]	11.4	48.6	146.
$\mu^\pm$ [d]	0.21	3.61	14.0
γ	17.8	126.	84.5
$e^\pm$ [d]	3.18	29.0	28.0
Total	43.7	344.	395.

Total Leakage = 782. MeV

(Binding energy + ν energy) = 229. MeV

Electromagnetic Source Energy = 943. MeV

a. CH_2, ρ = 0.87 g/cm^3; 254 cm in diameter, 355.6 cm in length.
b. kB = 0.01 (g/cm^2)/MeV.
c. Assumed to deposit their energy at their point of origin.
d. Includes rest mass energy.

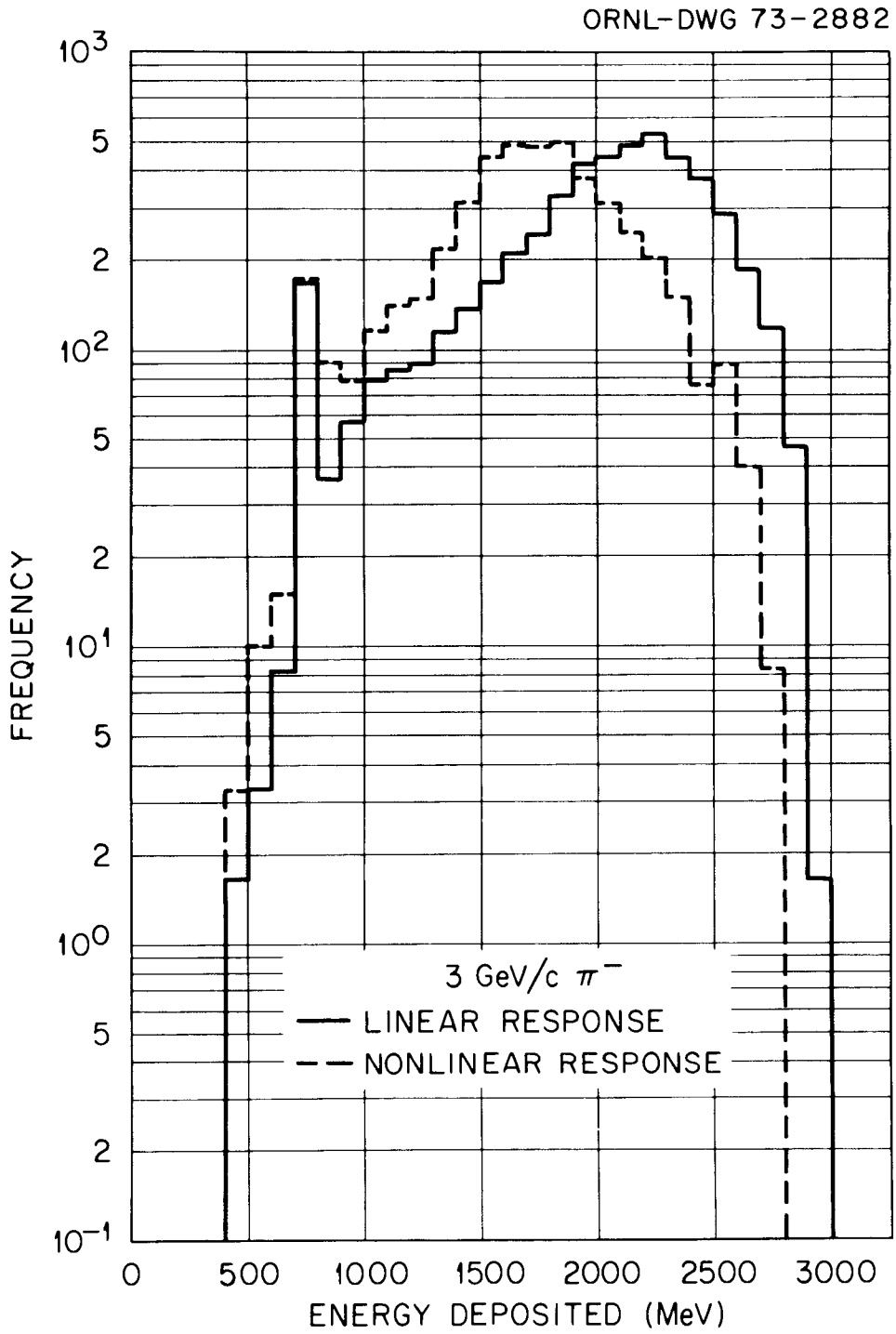

Fig. 18. Linear and nonlinear scintillation pulse-height distributions for incident 3-GeV/c π^-.

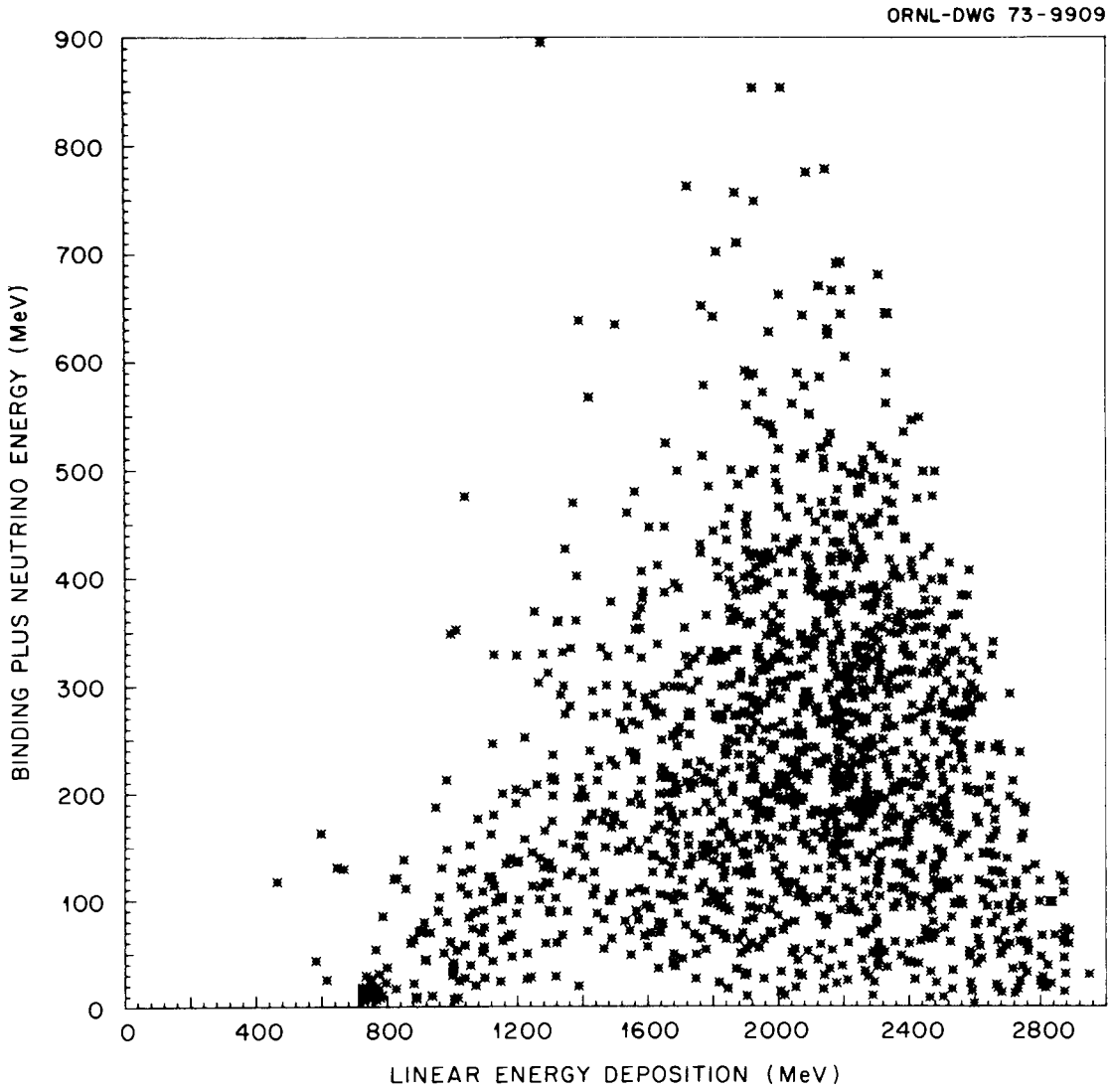

Fig. 19. Scatter plot of binding plus neutrino energy vs linear energy deposition for incident 3-GeV/c π^-.

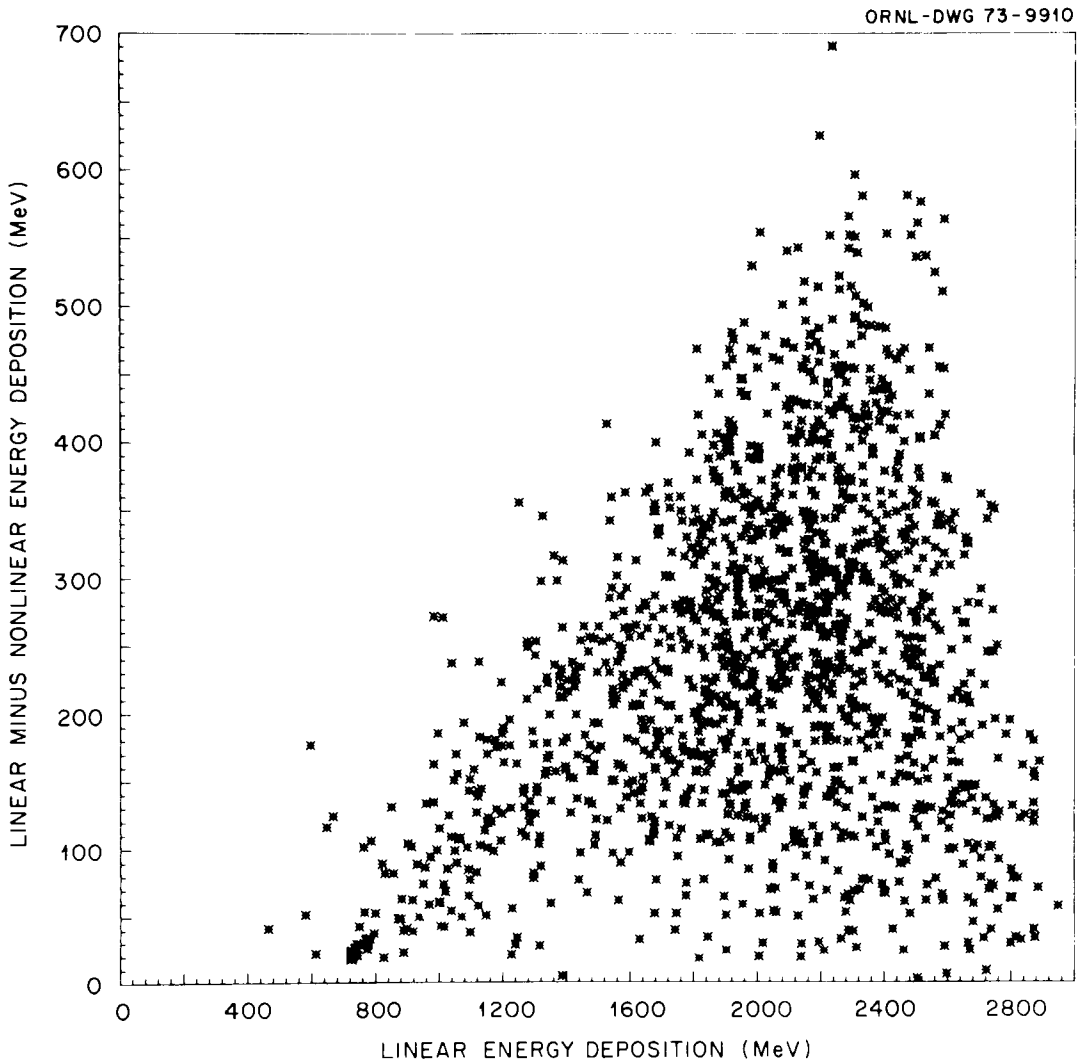

Fig. 20. Scatter plot of linear minus nonlinear energy deposition vs linear energy deposition for incident 3-GeV/c π^-.

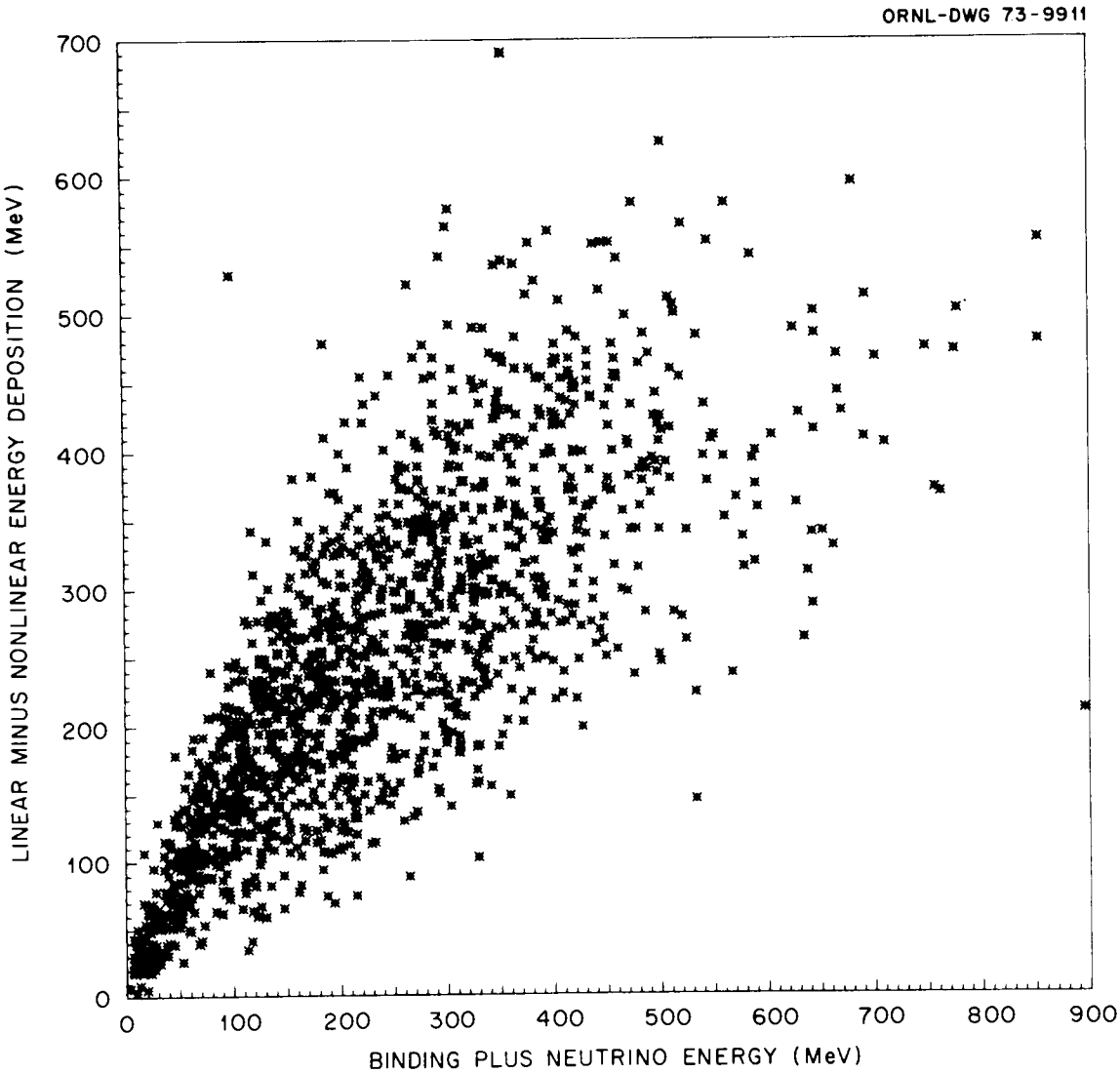

Fig. 21. Scatter plot of linear minus nonlinear energy deposition vs binding plus neutrino energy for incident 3-GeV/c π^-.

Table 8

Energy Deposition and Leakage Produced by the Interaction of 1-GeV/c Protons in a Large Scintillation Spectrometer[a]

	Energy Deposition (MeV)	
	Linear	Nonlinear[b]
Primary ionization	240.	225.
Secondary proton ionization	147.	122.
Secondary $\pi^{\pm}$ ionization	0.57	0.54
Secondary $\mu^{\pm}$ ionization	0.044	0.041
Nuclear recoil and evaporated charged particles other than protons[c]	8.76	0.88
Excitation energy following evaporation[c]	3.08	3.08
Neutrons with energy < 15 MeV[c]	5.59	2.39
Electromagnetic from the decay of π^{o}'s	1.34	1.34
Electromagnetic from the decay of $\mu^{\pm}$'s	0.29	0.29
Total Deposition	406.	356.

	Leakage Energy (MeV)		
	Front	Side	Back
p	0.	0.16	0.013
n	1.12	7.49	0.34
$\pi^{\pm}$ d	0.	0.	0.068
$\mu^{\pm}$ d	0.	0.	0.
Total	1.12	7.65	0.42

Total Leakage = 9.19 MeV

(Binding energy + ν energy) = 17.9 MeV

Electromagnetic Source Energy = 1.63 MeV

a. CH_2, ρ = 0.87 g/cm^3; 254 cm in diameter, 355.6 cm in length.
b. kB = 0.01 (g/cm^2)/MeV.
c. Assumed to deposit their energy at their point of origin.
d. Includes rest mass energy.

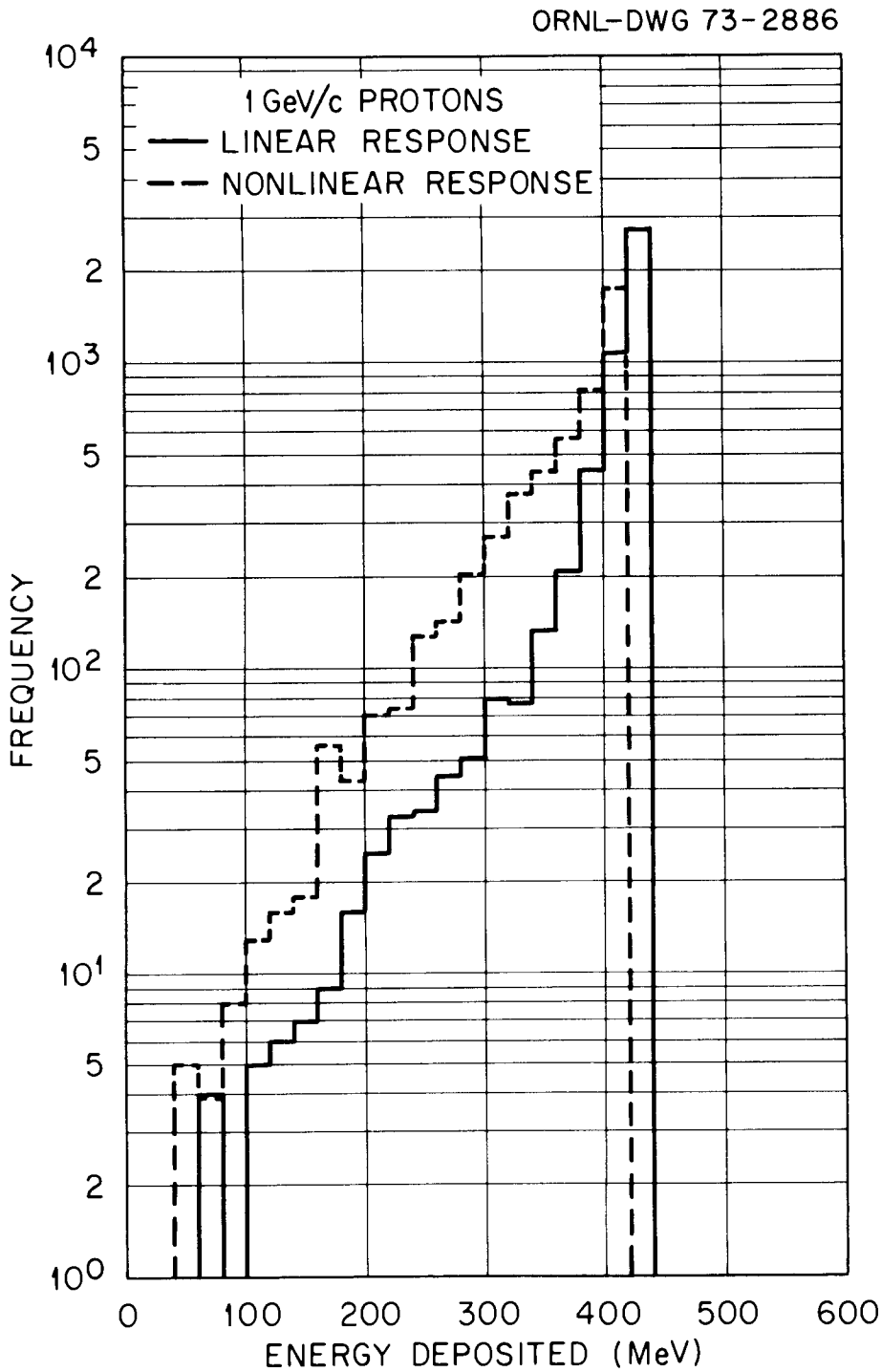

Fig. 22. Linear and nonlinear scintillation pulse-height distributions for incident 1-GeV/c protons.

nuclear interaction. Similar data for 3-GeV/c incident protons are given in tables 9 and 10 and in figs. 23-26.

A summary of the spatial energy dependence for the 3-GeV/c proton and π^- cases and the 1-GeV/c π^+ and π^- cases is presented in fig. 27. The figure shows the integral rate of energy containment as a function of depth in the spectrometer integrated over all radial intervals and the integral rate of energy containment as a function of radius integrated over all depths.

The 24-layer iron-plastic spectrometer is composed of 12 iron plates with individual thicknesses of 3.81 cm and of 12 plastic ($CH_{1.125}$, ρ = 1.05 g/cm^3) plates (sandwiched between the iron plates) with individual thicknesses of 0.476 cm. The diameter of both the iron and plastic sheets is 121.92 cm. The total gram thickness ($\sim$ 350 g/cm^2) of this device is comparable to the total gram thickness ($\sim$ 310 g/cm^2) of the all-liquid spectrometer already discussed. As before, the beam is assumed to enter at the center of and perpendicular to the front face.

The radially integrated energy deposition for 1-GeV/c π^- incident on the iron-plastic spectrometer is given in table 11. The low-energy-neutron cutoff for this series of calculations was reduced to 10 MeV. The spatially integrated energy deposition (in several categories) and the leakage energy (as to particle type and region of escape) are given in table 12. A MORSE calculation for this case indicated that 14% of the available low-energy-neutron energy will leak out. The linear and nonlinear energy deposition in the plastic only is also included in this table. It is rather obvious that the average amount of viewable energy deposited has been greatly reduced as compared to the similar 1-GeV/c π^- case for the all-liquid scintillation spectrometer.

TABLE 9

SPATIAL ENERGY DEPOSITION IN A LARGE SCINTILLATION SPECTROMETER

TYPE OF INCIDENT PARTICLE PROTONS
MOMENTUM OF INCIDENT PARTICLE 3 GEV/C

ENERGY DEPOSITION
(MEV/CM**3)

DEPTH IN SPECTROMETER (CM)	RADIAL INTERVAL (CM) 0 TO 10	10 TO 20	20 TO 30	30 TO 40	40 TO 50	50 TO 60
0 TO 20	1.02E-02	3.30E-04	8.33E-05	4.27E-05	2.15E-05	1.45E-05
	1.6	4.9	6.0	12.4	7.4	8.6
20 TO 40	1.09E-02	7.23E-04	2.29E-04	9.02E-05	4.99E-05	2.62E-05
	1.6	3.0	3.2	4.5	3.1	9.1
40 TO 60	1.06E-02	1.07E-03	3.34E-04	1.50E-04	7.91E-05	4.29E-05
	1.8	2.4	3.9	4.3	5.2	6.4
60 TO 80	9.04E-03	1.18E-03	4.56E-04	2.01E-04	9.44E-05	5.89E-05
	1.7	3.4	3.3	4.3	5.4	4.3
80 TO 100	8.06E-03	1.27E-03	5.04E-04	2.51E-04	1.33E-04	7.01E-05
	1.7	1.5	2.4	5.7	6.5	3.2
100 TO 120	6.49E-03	1.29E-03	5.13E-04	2.76E-04	1.47E-04	9.03E-05
	1.2	3.2	4.2	4.0	6.4	6.4
120 TO 140	5.47E-03	1.22E-03	5.07E-04	2.90E-04	1.55E-04	9.36E-05
	2.7	1.7	2.4	4.4	4.1	3.9
140 TO 160	4.46E-03	1.12E-03	5.22E-04	2.44E-04	1.64E-04	1.01E-04
	3.1	2.9	3.5	4.6	4.6	4.0
160 TO 180	3.66E-03	9.96E-04	4.83E-04	2.61E-04	1.63E-04	1.02E-04
	3.7	3.8	3.6	2.8	4.8	3.7
180 TO 200	2.80E-03	8.28E-04	4.51E-04	2.55E-04	1.46E-04	9.30E-05
	4.5	2.7	2.6	4.7	3.4	3.7
200 TO 220	2.22E-03	7.26E-04	3.85E-04	2.27E-04	1.35E-04	1.03E-04
	3.8	3.9	4.1	3.4	5.6	4.5
220 TO 240	1.79E-03	5.95E-04	3.27E-04	2.17E-04	1.37E-04	9.02E-05
	3.4	2.4	3.8	4.6	5.8	5.7
240 TO 260	1.37E-03	4.97E-04	2.81E-04	1.84E-04	1.27E-04	8.59E-05
	4.6	5.6	4.2	3.3	4.8	9.3
260 TO 280	1.15E-03	4.54E-04	2.59E-04	1.55E-04	1.12E-04	6.93E-05
	6.8	5.4	3.8	4.9	4.9	6.5
280 TO 300	8.63E-04	3.56E-04	2.19E-04	1.37E-04	9.62E-05	6.99E-05
	9.5	4.8	3.7	5.0	3.8	5.7
300 TO 325	6.60E-04	2.83E-04	1.83E-04	1.15E-04	8.16E-05	5.60E-05
	5.9	6.3	4.8	5.4	6.6	5.1
325 TO 356	4.15E-04	1.92E-04	1.28E-04	9.54E-05	6.60E-05	4.88E-05
	7.1	3.9	5.8	4.9	5.1	7.8

TABLE 9 (CONT'D)

SPATIAL ENERGY DEPOSITION IN A LARGE SCINTILLATION SPECTROMETER

TYPE OF INCIDENT PARTICLE PROTONS
MOMENTUM OF INCIDENT PARTICLE 3 GEV/C

ENERGY DEPOSITION
(MEV/CM**3)

DEPTH IN SPECTROMETER (CM)	RADIAL INTERVAL (CM) 60 TO 70	70 TO 80	80 TO 90	90 TO 100	100 TO 110	110 TO 127
0 TO 20	9.37E-06	7.49E-06	5.24E-06	3.73E-06	2.41E-06	1.96E-06
	8.6	10.5	14.0	14.1	15.8	8.8
20 TO 40	1.65E-05	1.02E-05	8.45E-06	4.96E-06	4.32E-06	3.07E-06
	8.9	10.0	9.6	11.4	8.8	8.9
40 TO 60	2.15E-05	1.42E-05	9.35E-06	6.41E-06	5.13E-06	3.43E-06
	5.7	9.5	14.8	10.4	7.5	10.8
60 TO 80	3.38E-05	2.26E-05	1.34E-05	9.36E-06	7.03E-06	5.01E-06
	8.4	11.8	7.3	7.5	11.5	8.7
80 TO 100	4.74E-05	2.97E-05	2.06E-05	1.35E-05	9.39E-06	6.69E-06
	6.2	2.7	9.8	7.2	10.2	2.6
100 TO 120	5.01E-05	3.57E-05	2.33E-05	1.67E-05	1.17E-05	7.80E-06
	5.9	8.4	5.4	3.9	7.1	5.5
120 TO 140	6.07E-05	4.09E-05	2.73E-05	1.97E-05	1.45E-05	9.71E-06
	5.5	6.9	6.8	6.6	7.6	5.6
140 TO 160	6.00E-05	4.53E-05	2.98E-05	2.05E-05	1.58E-05	9.08E-06
	7.0	8.1	7.0	6.2	7.2	5.1
160 TO 180	7.39E-05	4.66E-05	3.25E-05	2.28E-05	1.76E-05	1.15E-05
	4.7	5.5	6.5	9.1	6.1	7.2
180 TO 200	6.22E-05	4.94E-05	2.94E-05	2.34E-05	1.80E-05	1.28E-05
	2.8	5.2	7.7	4.4	9.2	6.0
200 TO 220	6.15E-05	4.25E-05	3.56E-05	2.35E-05	1.55E-05	1.11E-05
	5.1	7.0	4.1	5.2	5.6	6.8
220 TO 240	6.02E-05	4.40E-05	3.01E-05	2.08E-05	1.75E-05	1.08E-05
	5.5	5.4	8.5	9.5	6.7	5.7
240 TO 260	5.83E-05	4.21E-05	2.53E-05	2.26E-05	1.64E-05	1.20E-05
	6.5	9.8	6.6	6.8	7.1	5.1
260 TO 280	4.83E-05	3.29E-05	3.00E-05	2.09E-05	1.41E-05	1.03E-05
	5.4	6.9	5.9	11.4	10.5	4.8
280 TO 300	4.85E-05	3.43E-05	2.34E-05	1.65E-05	1.38E-05	9.81E-06
	6.2	7.8	5.5	7.8	8.4	5.6
300 TO 325	4.52E-05	2.89E-05	2.13E-05	2.00E-05	1.51E-05	1.08E-05
	6.2	6.4	6.7	7.7	9.1	7.9
325 TO 356	3.34E-05	2.31E-05	1.84E-05	1.48E-05	1.18E-05	8.43E-06
	3.2	6.8	6.2	5.2	6.4	6.6

Table 10

Energy Deposition and Leakage Produced by the Interaction of 3-GeV/c Protons in a Large Scintillation Spectrometer[a]

Energy Deposition (MeV)	Linear	Nonlinear[b]
Primary ionization	137.	134.
Secondary proton ionization	871.	742.
Secondary $\pi^{\pm}$ ionization	156.	151.
Secondary $\mu^{\pm}$ ionization	7.59	7.28
Nuclear recoil and evaporated charged particles other than protons[c]	67.5	9.70
Excitation energy following evaporation[c]	17.6	17.6
Neutrons with energy < 15 MeV[c]	42.8	18.4
Electromagnetic from the decay of π°'s	217.	217.
Electromagnetic from the decay of $\mu^{\pm}$'s	22.2	22.2
Total Deposition	1539.	1318.

Leakage Energy (MeV)	Front	Side	Back
p	0.32	12.9	101.
n	5.56	88.3	114.
$\pi^{\pm}$ [d]	3.00	5.59	12.2
$\mu^{\pm}$ [d]	0.070	0.47	0.70
γ	10.5	47.9	19.8
$e^{\pm}$ [d]	1.64	9.79	5.28
Total	21.1	165.	253.

Total Leakage = 439. MeV

(Binding energy + ν energy) = 221. MeV

Electromagnetic Source Energy = 335. MeV

a. CH_2, ρ = 0.87 g/cm^3; 254 cm in diameter, 355.6 cm in length.
b. kB = 0.01 (g/cm^2)/MeV.
c. Assumed to deposit their energy at their point of origin.
d. Includes rest mass energy.

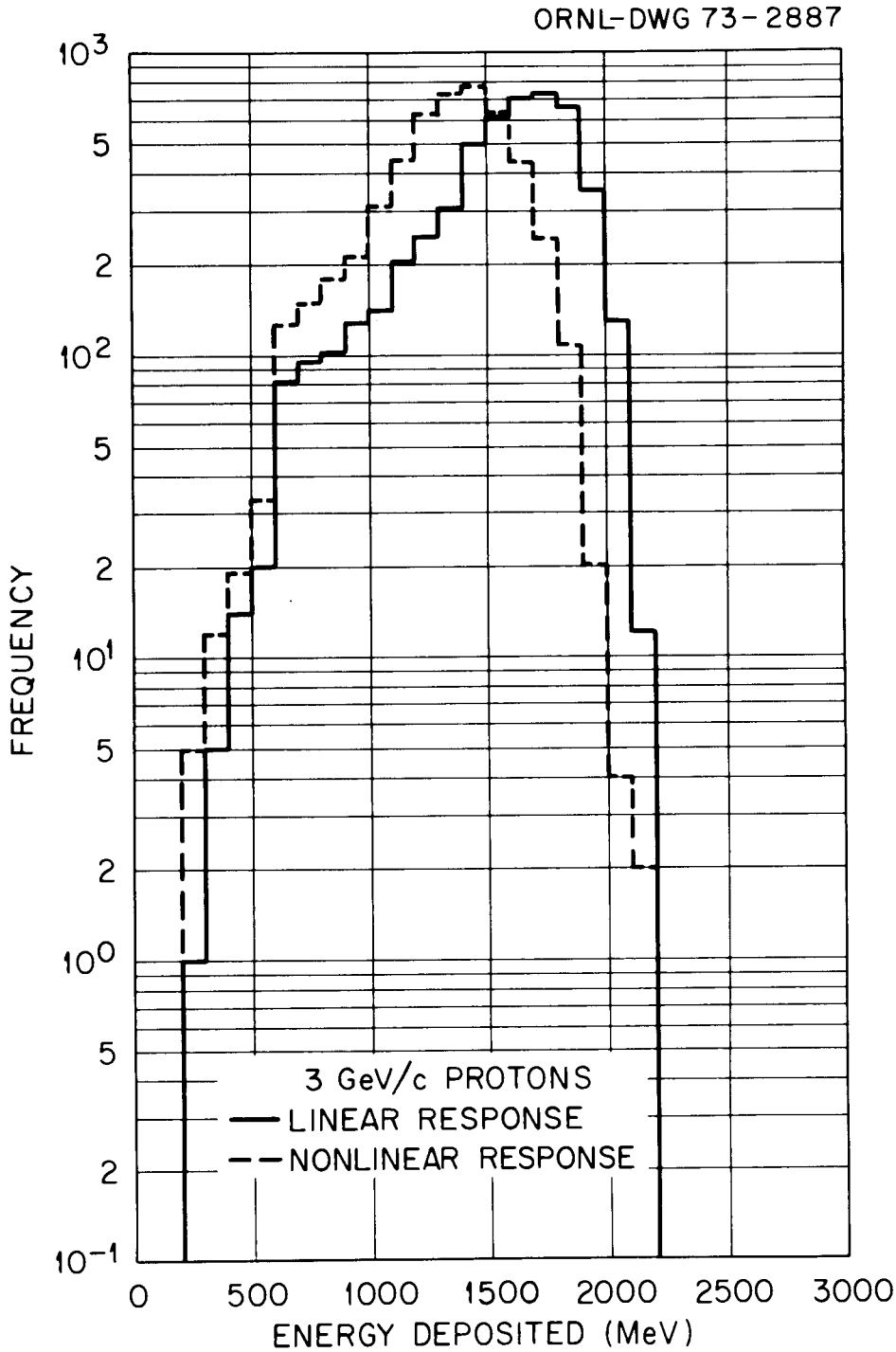

Fig. 23. Linear and nonlinear scintillation pulse-height distributions for incident 3-GeV/c protons.

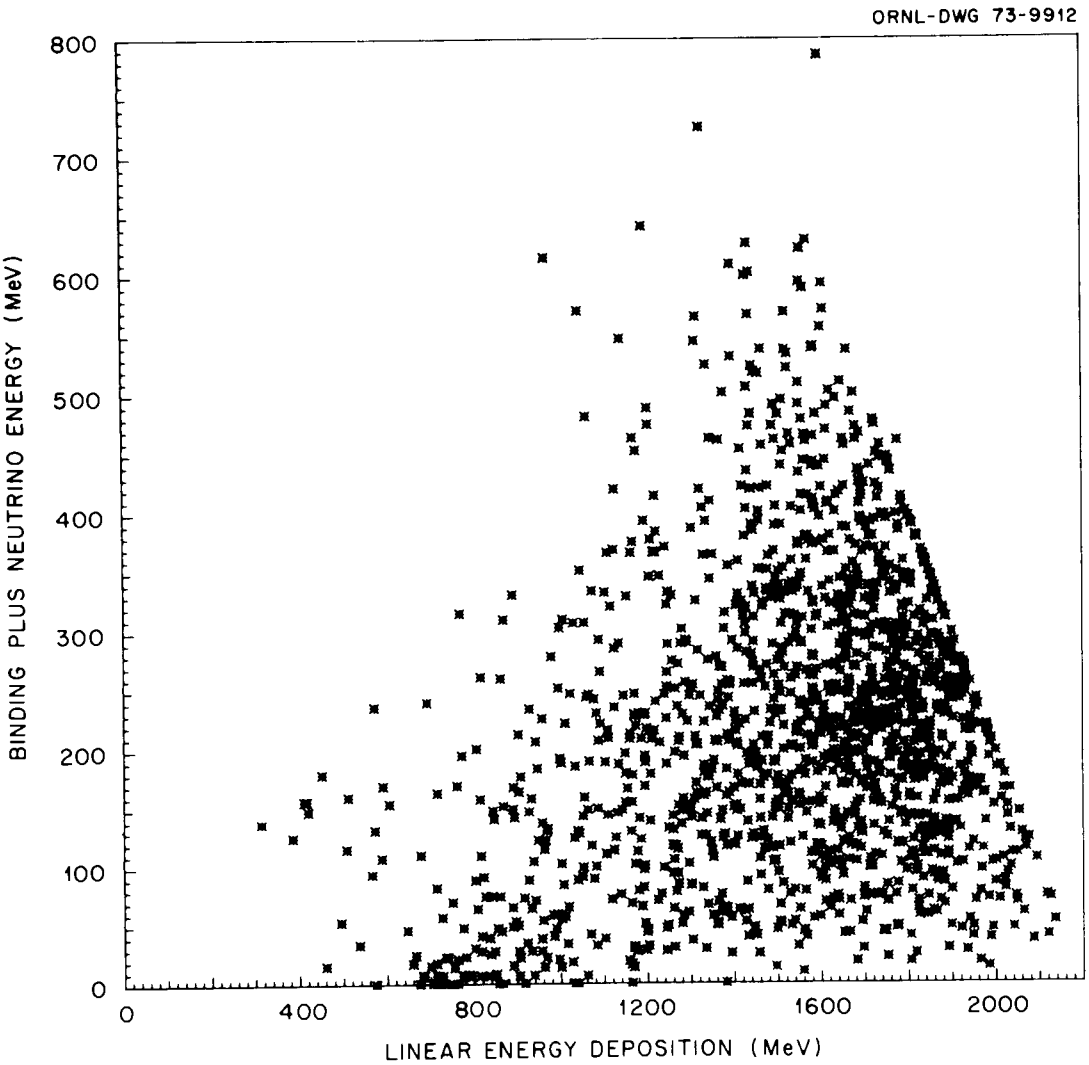

Fig. 24. Scatter plot of binding plus neutrino energy vs linear energy deposition for incident 3-GeV/c protons.

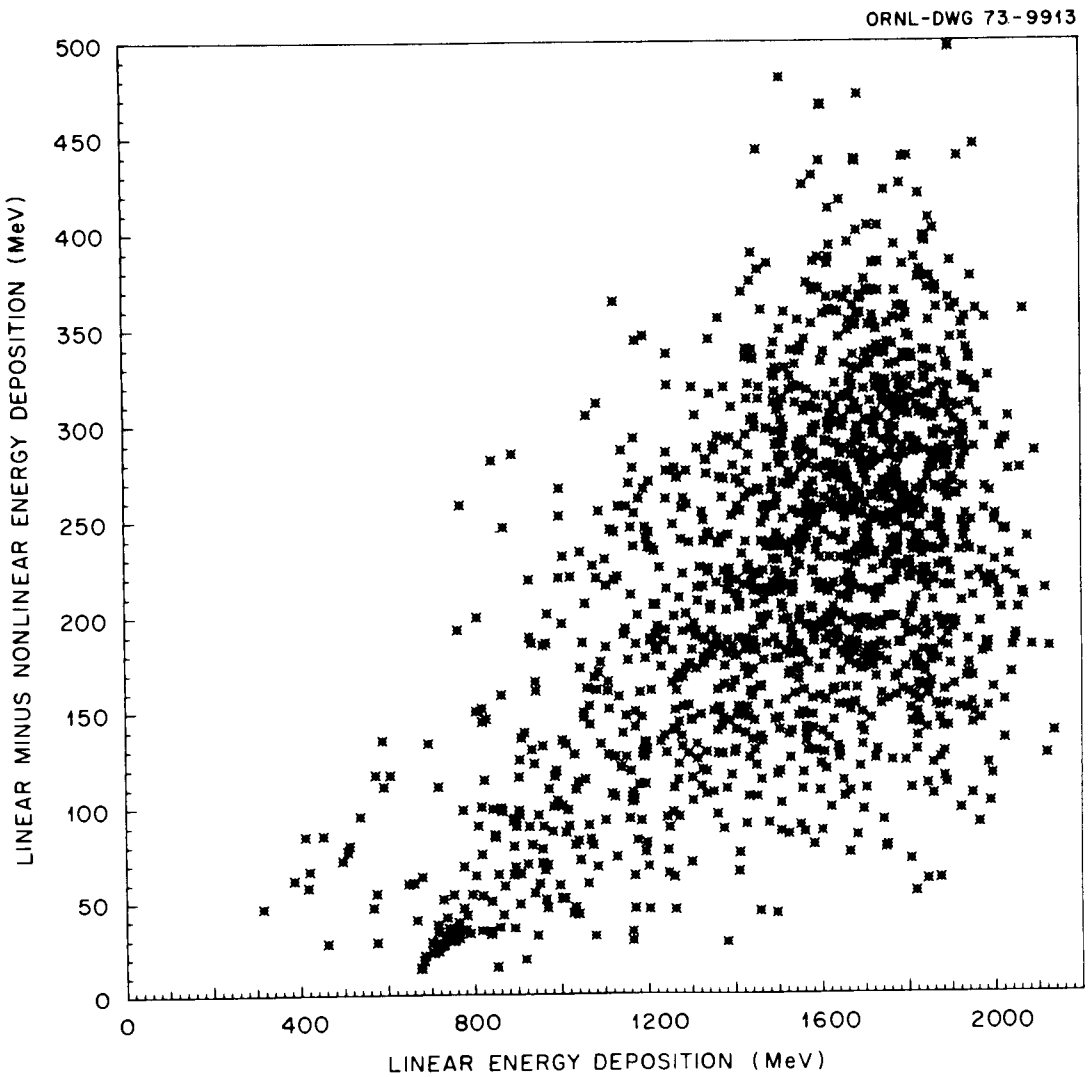

Fig. 25. Scatter plot of linear minus nonlinear energy deposition vs linear energy deposition for incident 3-GeV/c protons.

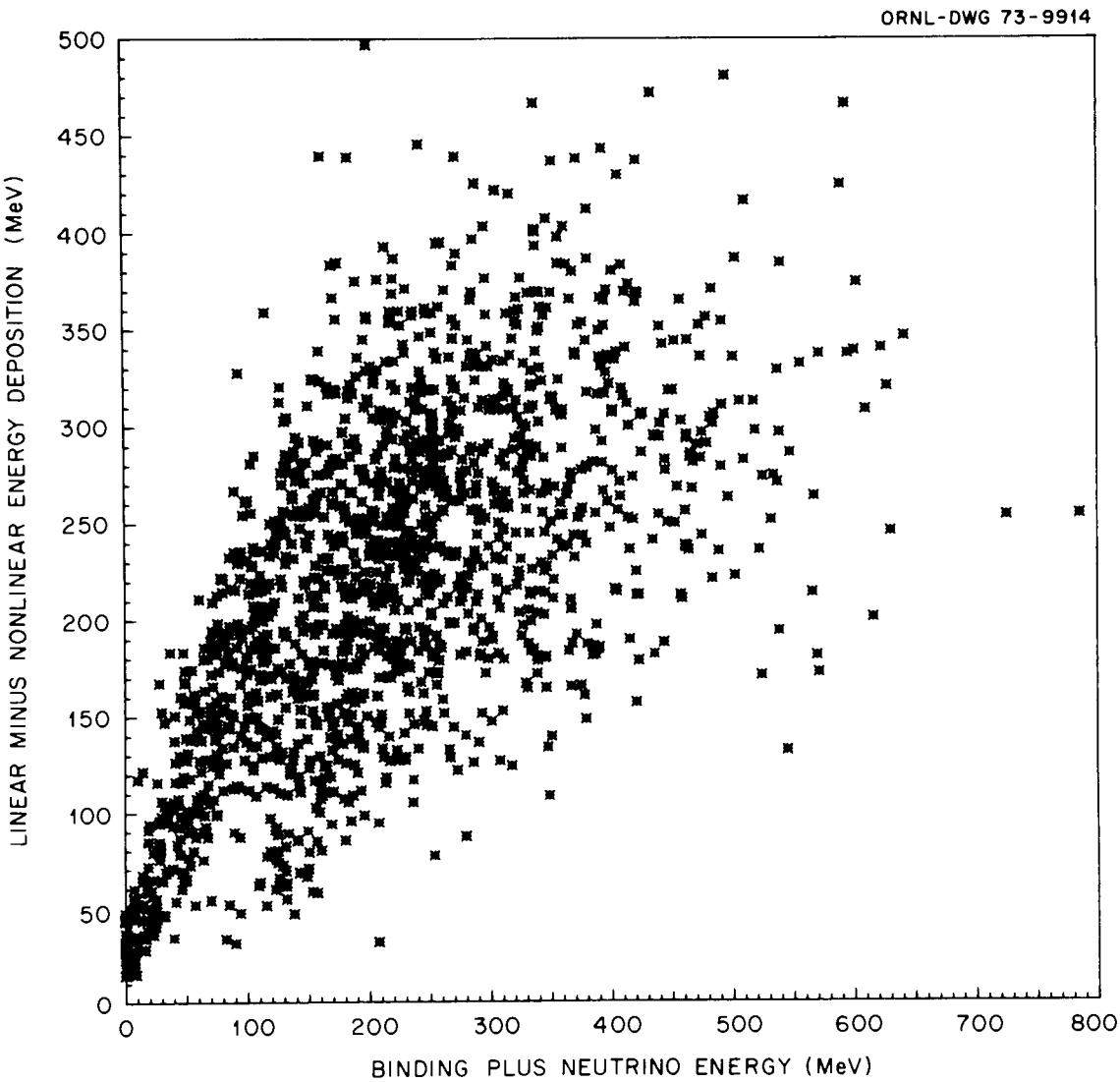

Fig. 26. Scatter plot of linear-nonlinear energy deposition vs binding plus neutrino energy for incident 3-GeV/c protons.

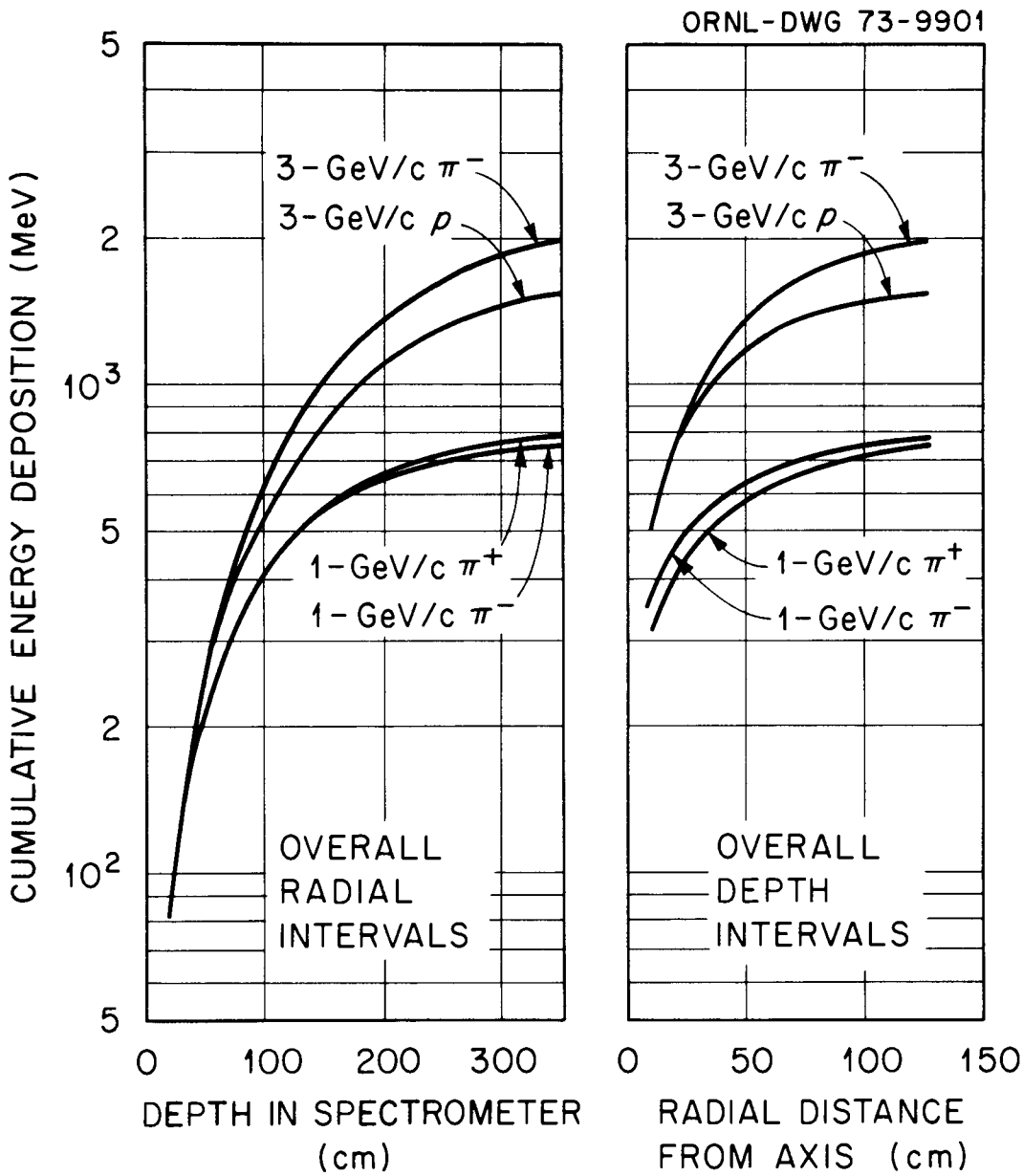

Fig. 27. Cumulative energy deposition vs depth and radius for the various particle types and particle energies.

Table 11

Spatial Energy Deposition Produced by the Interaction of 1-GeV/c π^- in a 24-Layer Iron-Plastic Spectrometer

Depth Interval (cm)	Energy Deposition (MeV/cm)
0. - 3.810	27.3
3.810 - 4.286	5.47
4.286 - 8.096	28.4
8.096 - 8.572	5.36
8.572 - 12.38	25.5
12.38 - 12.86	4.62
12.86 - 16.67	21.2
16.67 - 17.14	4.32
17.14 - 20.95	17.7
20.95 - 21.43	3.29
21.43 - 25.24	14.7
25.24 - 25.72	2.96
25.72 - 29.53	11.5
29.53 - 30.00	2.41
30.00 - 33.81	9.31
33.81 - 34.29	1.99
34.29 - 38.10	7.63
38.10 - 38.58	1.31
38.58 - 42.39	5.98
42.39 - 42.86	1.34
42.86 - 46.67	4.60
46.67 - 47.15	0.804
47.15 - 50.96	3.61
50.96 - 51.44	0.528

Table 12

Energy Deposition and Leakage Produced by the Interaction of 1-GeV/c π^- in a 24-Layer Iron-Plastic Spectrometer[a]

Energy Deposition (MeV)	Iron and Plastic	Plastic Linear	Plastic Nonlinear[b]
Primary ionization	197.	3.66	3.59
Secondary proton ionization	193.	5.35	3.85
Secondary $\pi^\pm$ ionization	88.5	1.95	1.89
Secondary $\mu^\pm$ ionization	2.22	0.050	0.049
Nuclear recoil and evaporated charged particles other than protons[c]	20.2	1.32	0.16
Excitation energy following evaporation[c]	38.3	0.60	0.60
Neutrons with energy < 10 MeV[c]	40.1	1.06	0.42
Electromagnetic from the decay of π°'s	116.	2.39	2.39
Electromagnetic from the decay of $\mu^\pm$'s	0.12	0.003	0.003
Total Deposition	696.	16.4	13.0

Leakage Energy (MeV)	Front	Side	Back
p	0.84	0.044	0.58
n	17.0	4.04	25.2
$\pi^\pm$ d	6.95	0.	36.3
$\mu^\pm$ d	0.	0.	1.19
γ	5.72	0.0066	1.41
$e^\pm$ d	1.52	0.	0.29
Total	32.0	4.09	65.0

Total Leakage = 101. MeV

(Binding energy + ν energy) = 202. MeV

Electromagnetic Source Energy = 127. MeV

a. Fe: 3.81-cm thick; plastic ($CH_{1.125}$, ρ = 1.05 g/cm^3): 0.476-cm thick; spectrometer: 121.92 cm in diameter.
b. kB = 0.01 (g/cm^2)/MeV.
c. Assumed to deposit their energy at their point of origin.
d. Includes rest mass energy.

The linear and nonlinear pulse-height distributions are given in fig. 28. The large peak at 12.5 MeV is due primarily to those incident particles which transverse the device without interacting. Due to the relatively small amount of energy which is sampled, the resolution of this device for 1-GeV/c π^- is poor — $\sim$ 100%. Also, the slowly decreasing high-energy tail could cause problems if this device were to be used to measure a hadron spectrum which is decreasing very rapidly with increasing energy. The expected Cerenkov pulse-height distribution is given in fig. 29, and the average contributors to this distribution are given in table 13.

The same type of data presented for the 1-GeV/c incident π^- is given for 3-GeV/c incident π^- in tables 14-16 and in figs. 30 and 31. The scintillation pulse-height distribution in fig. 30 has a better-defined shape than that for the 1-GeV/c π^- case, but still the resolution is poor due to the small amount of sampled light.

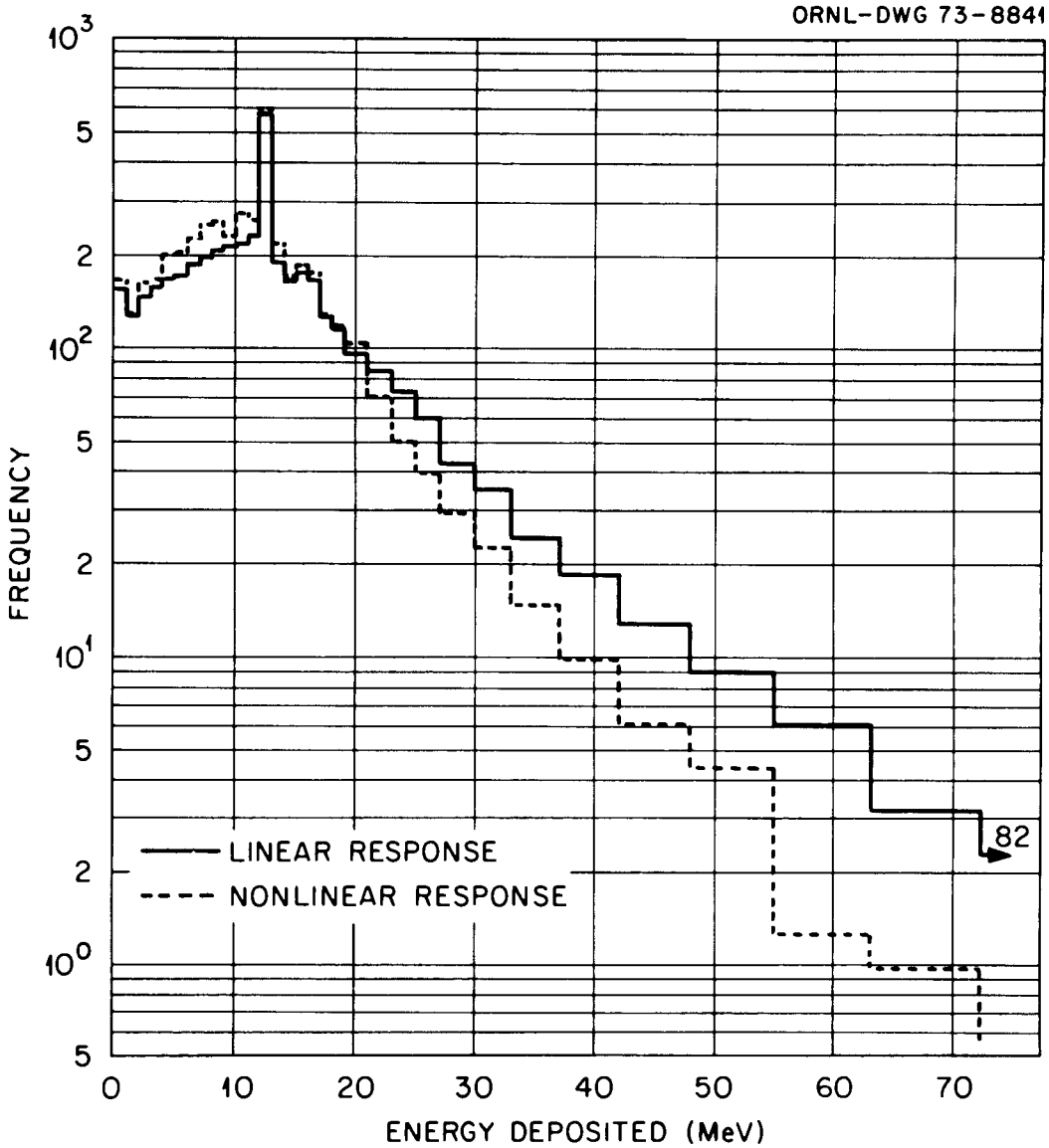

Fig. 28. Linear and nonlinear scintillation pulse-height distributions for incident 1-GeV/c π^-.

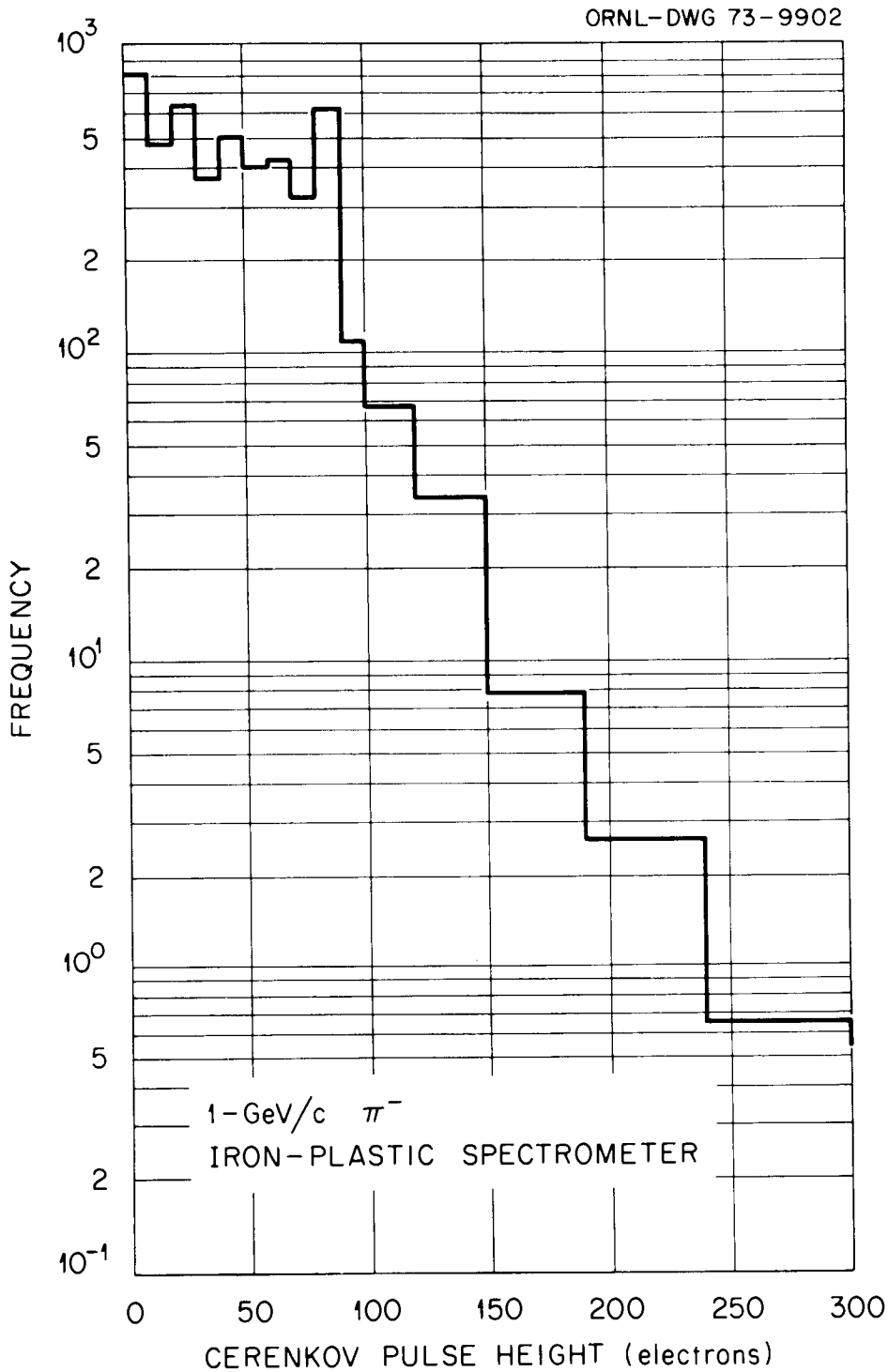

Fig. 29. Cerenkov pulse-height distribution for incident 1-GeV/c π^-.

Table 13

Average Cerenkov Pulse from the Interaction of 1-GeV/c π^- in a 24-Layer Iron-Plastic Spectrometer

	Cerenkov Pulse (electrons)
Primary	26.5
Secondary protons	0.12
Secondary charged pions	8.51
Secondary muons	0.29
Electromagnetic cascade	14.1
TOTAL	49.5

Table 14

Spatial Energy Deposition Produced by the Interaction of 3-GeV/c π^- in a 24-Layer Iron-Plastic Spectrometer

Depth Interval (cm)	Energy Deposition (MeV/cm)
0. - 3.810	40.5
3.810 - 4.286	9.45
4.286 - 8.096	51.3
8.096 - 8.572	10.9
8.572 - 12.38	55.9
12.38 - 12.86	11.1
12.86 - 16.67	55.9
16.67 - 17.14	10.7
17.14 - 20.95	53.1
20.95 - 21.43	9.69
21.43 - 25.24	47.3
25.24 - 25.72	8.83
25.72 - 29.53	42.8
29.53 - 30.00	8.06
30.00 - 33.81	37.7
33.81 - 34.29	7.31
34.29 - 38.10	32.0
38.10 - 38.58	6.02
38.58 - 42.39	26.7
42.39 - 42.86	4.92
42.86 - 46.67	22.7
46.67 - 47.15	4.27
47.15 - 50.96	17.8
50.96 - 51.44	3.31

Table 15

Energy Deposition and Leakage Produced by the Interaction of 3-GeV/c π^- in a 24-Layer Iron-Plastic Spectrometer[a]

Energy Deposition (MeV)

	Iron and Plastic	Plastic	
		Linear	Nonlinear[b]
Primary ionization	221.	4.14	4.05
Secondary proton ionization	648.	16.8	12.7
Secondary $\pi^\pm$ ionization	248.	5.43	5.26
Secondary $\mu^\pm$ ionization	1.34	0.034	0.033
Nuclear recoil and evaporated charged particles other than protons[c]	57.3	2.88	0.35
Excitation energy following evaporation[c]	88.9	1.40	1.40
Neutrons with energy < 10 MeV[c]	92.9	2.51	0.99
Electromagnetic from the decay of π^0's	529.	11.8	11.8
Electromagnetic from the decay of $\mu^\pm$'s	0.34	0.011	0.011
Total Deposition	1887.	45.0	36.6

Leakage Energy (MeV)

	Front	Side	Back
p	1.87	0.12	30.1
n	39.0	12.7	167.
$\pi^\pm$ [d]	15.1	0.	279.
$\mu^\pm$ [d]	0.032	0.	1.69
γ	7.85	0.012	18.2
$e^\pm$ [d]	1.89	0.0064	5.57
Total	65.7	12.8	502.

Total Leakage = 580. MeV

(Binding energy + ν energy) = 534. MeV

Electromagnetic Source Energy = 565. MeV

a. Fe: 3.81-cm thick; plastic ($CH_{1.125}$, ρ = 1.05 g/cm^3): 0.476-cm thick; spectrometer: 121.92 cm in diameter.
b. kB = 0.01 (g/cm^2)/MeV.
c. Assumed to deposit their energy at their point of origin.
d. Includes rest mass energy.

Table 16

Average Cerenkov Pulse from the Interaction of 3-GeV/c π^- in a 24-Layer Iron-Plastic Spectrometer

	Cerenkov Pulse (electrons)
Primary	26.4
Secondary protons	2.90
Secondary charged pions	25.9
Secondary muons	0.13
Electromagnetic cascade	64.4
TOTAL	120.

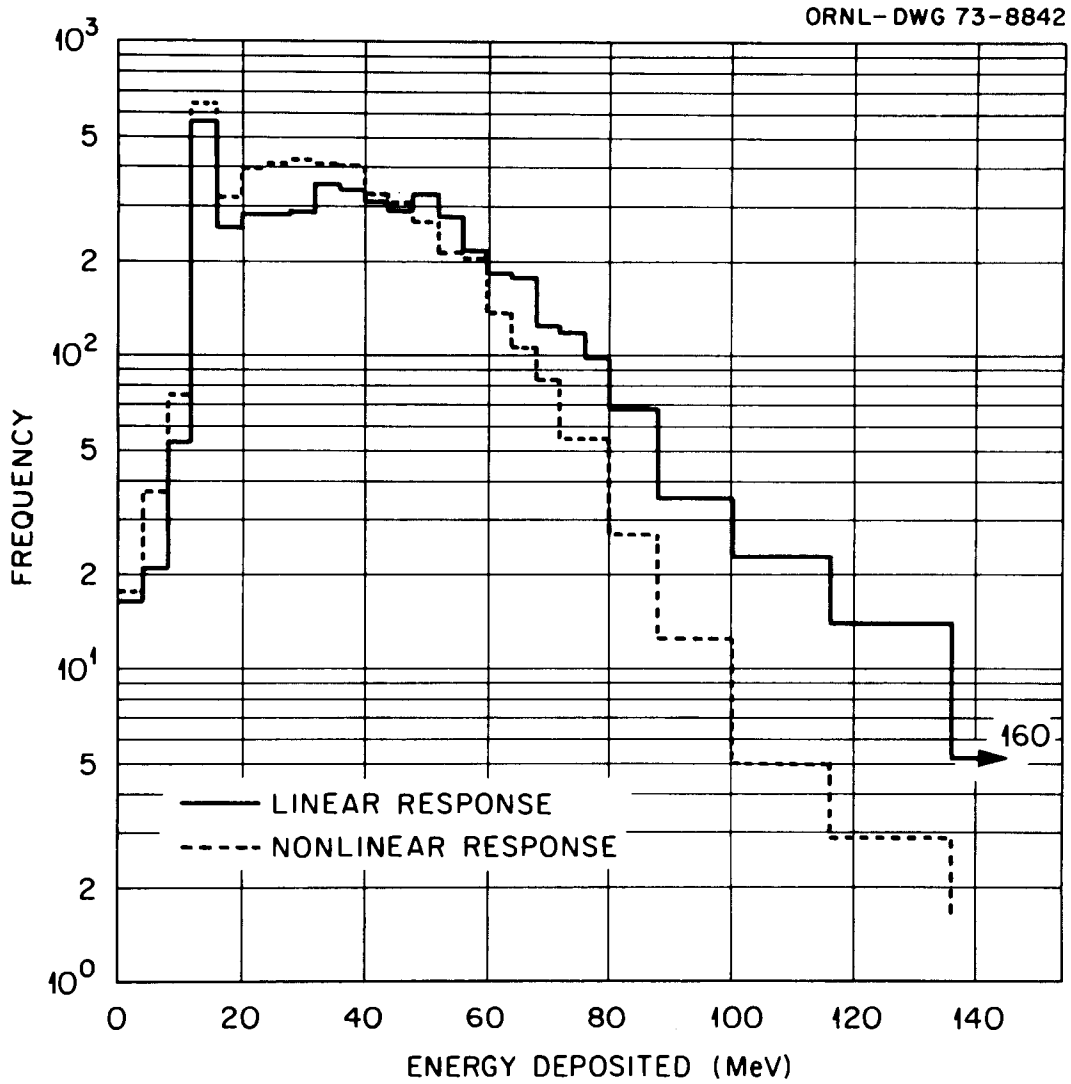

Fig. 30. Linear and nonlinear scintillation pulse-height distributions for incident 3-GeV/c π^-.

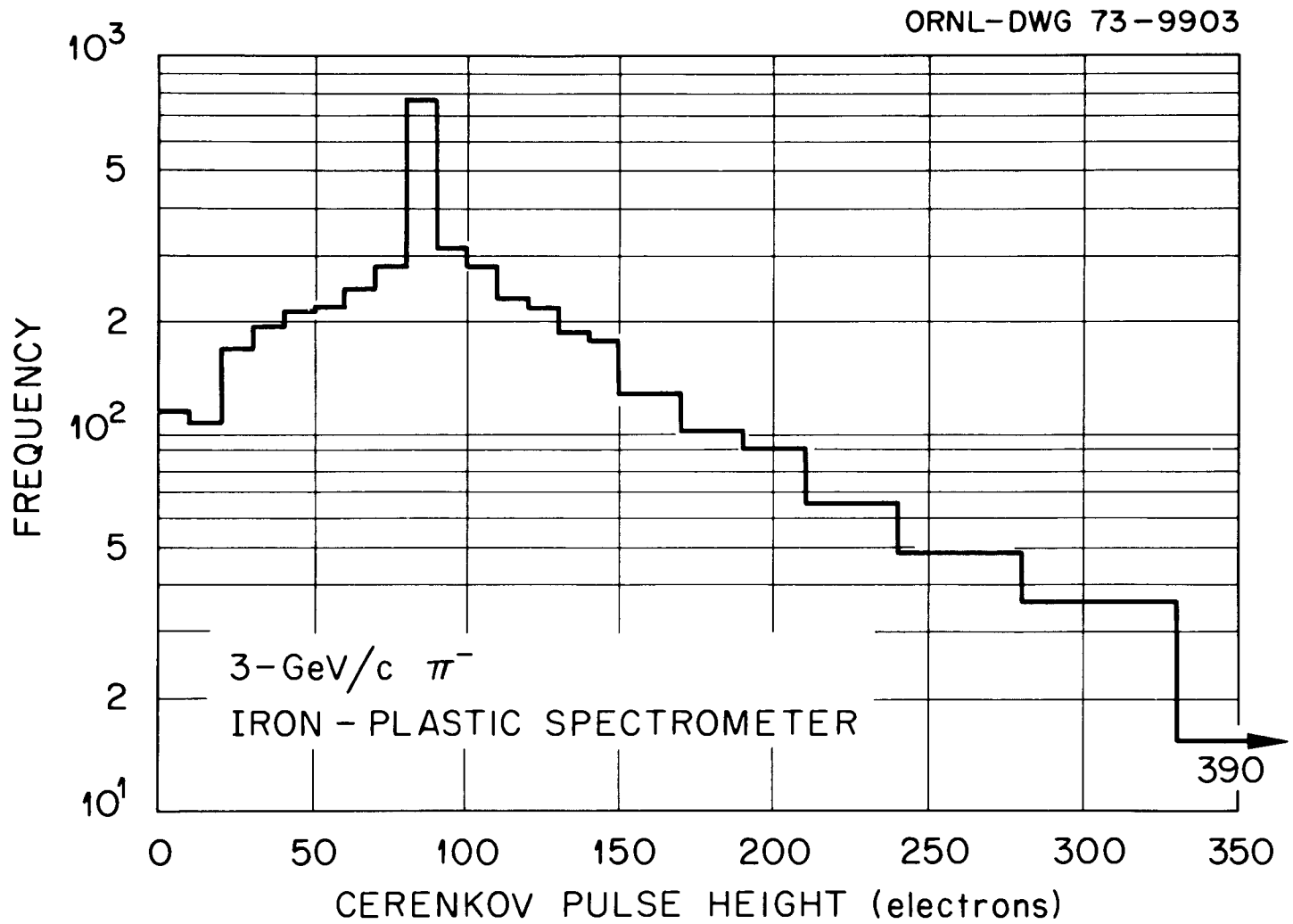

Fig. 31. Cerenkov pulse-height distribution for incident 3-GeV/c π^-.

ACKNOWLEDGMENTS

The authors wish to thank Dr. W. J. Willis of the Brookhaven National Laboratory and Dr. W. Selove of the University of Pennsylvania for pointing out the need for such calculations and for many helpful and enlightening discussions. Thanks are also due Dr. R. G. Alsmiller, Jr. of the Oak Ridge National Laboratory for his advice and helpful comments.

REFERENCES

1) T. A. Gabriel and K. C. Chandler, Energy deposition and energy-deposition fluctuations in an ionization spectrometer and a total-absorption nuclear-cascade counter, Oak Ridge Nat. Lab. Report ORNL-TM-4118 (1973); to be published in Particle Accelerators.

2) J. B. Birks, The Theory and Practice of Scintillation Counting, (The Macmillan Company, New York, 1964).

3) K. C. Chandler and T. W. Armstrong, Operating instructions for the high-energy nucleon-meson transport code HETC, Oak Ridge Nat. Lab. Report ORNL-4744 (1972).

4) H. W. Bertini, Phys. Rev. C6 (1972) 631.

5) T. A. Gabriel, R. G. Alsmiller, Jr., and M. P. Guthrie, An extrapolation method for predicting nucleon and pion differential production cross sections from high-energy (> 3 GeV) nucleon-nucleus collisions, Oak Ridge Nat. Lab. Report ORNL-4542 (1970).

6) Hugo W. Bertini, Miriam P. Guthrie, and Arline H. Culkowski, Phenomenologically determined isobar angular distributions for nucleon-nucleon and pion-nucleon reactions below 3 GeV, Oak Ridge Nat. Lab. Report ORNL-TM-3132 (1970).

7) T. A. Gabriel, R. T. Santoro, and J. Barish, A calculational method for predicting particle spectra from high-energy nucleon and pion collisions (≥ 3 GeV) with protons, Oak Ridge Nat. Lab. Report ORNL-TM-3615 (1971).

8) E. A. Straker *et al.*, The MORSE code - a multigroup neutron and gamma-ray Monte Carlo transport code, Oak Ridge Nat. Lab. Report ORNL-4585 (1970).

[9]) D. C. Irving *et al.*, O5R, a general-purpose Monte Carlo neutron transport code, Oak Ridge Nat. Lab. Report ORNL-3622 (1965).

[10]) H. L. Beck, A Monte Carlo simulation of the transport of high energy electrons and photons in matter, USAEC Health and Safety Lab. Report HASL-213 (1969).

[11]) T. W. Armstrong and K. C. Chandler, SPAR, a FORTRAN program for computing stopping powers and ranges for muons, charged pions, protons, and heavy ions, Oak Ridge Nat. Lab. Report ORNL-4869 (1973).

Internal Distribution

1-3. L. S. Abbott
4. F. S. Alsmiller
5. R. G. Alsmiller, Jr.
6-10. J. D. Amburgey
11. T. W. Armstrong
12. J. Barish
13. H. W. Bertini
14. A. A. Brooks
15. H. P. Carter
16. K. C. Chandler
17. G. T. Chapman
18. C. E. Clifford
19-53. T. A. Gabriel
54. T. A. Love
55. F. C. Maienschein
56. E. M. Oblow
57. R. W. Peelle
58. R. W. Roussin
59. RSIC
60. R. T. Santoro
61. D. Sundberg
62. J. E. Turner
63. G. E. Whitesides
64. H. A. Wright
65. R. Q. Wright
66. A. Zucker
67. H. Feshbach (consultant)
68. P. F. Fox (consultant)
69. C. R. Mehl (consultant)
70. H. T. Motz (consultant)
71-72. Central Research Library
73. ORNL Y-12 Technical Library, Document Reference Section
74-75. Laboratory Records Department
76. Laboratory Records ORNL RC
77. ORNL Patent Office

External Distribution

78. H. Goldstein, Columbia University, 287A Mudd Building, New York, New York, 10027.
79. P. B. Hemmig, Division of Reactor Research and Development, U. S. Atomic Energy Commission, Washington, D. C., 20545.
80. W. H. Hannum, Division of Reactor Research and Development, U. S. Atomic Energy Commission, Washington, D. C., 20545.
81. Kermit Laughon, AEC Site Representative.
82-188. Given AEC High-Energy Accelerator Shielding Distribution.*
189-190. Technical Information Center (TIC).
191. Research and Technical Support Division (ORO).

*This distribution list is available upon request.